SYNTHESIS AND STRUCTURAL CHARACTERIZATION OF Co-Al BASED SUPERALLOYS

A THESIS SUBMITTED TO
THE GRADUATE SCHOOL OF NATURAL AND APPLIED SCIENCES
OF
MIDDLE EAST TECHNICAL UNIVERSITY

BY

ALİ FIRAT DİNLER

IN PARTIAL FULFILLMENT OF THE REQUIREMENTS
FOR
THE DEGREE OF MASTER OF SCIENCE
IN
METALLURGICAL AND MATERIALS ENGINEERING

JUNE 2019

Approval of the Thesis:

SYNTHESIS AND STRUCTURAL CHARACTERIZATION OF Co-Al BASED SUPERALLOYS

submitted by **ALİ FIRAT DİNLER** in partial fulfillment of the requirements for the degree of **Master of Science in Metallurgical and Materials Engineering Department, Middle East Technical University** by,

Prof. Dr. Halil Kalıpçılar _____
Dean, Graduate School of **Natural and Applied Sciences**

Prof. Dr. C. Hakan Gür _____
Head of Department, **Metallurgical and Materials Eng, METU**

Prof. Dr. Amdulla O. Mekhrabov _____
Supervisor, **Metallurgical and Materials Eng. Dept, METU**

Prof. Dr. M. Vedat Akdeniz _____
Co-Supervisor, **Metallurgical and Materials Eng. Dept., METU**

Examining Committee Members

Prof. Dr. Amdulla O. Mekhrabov _____
Metallurgical and Materials Eng. Dept., METU

Prof. Dr. M. Vedat Akdeniz _____
Metallurgical and Materials Eng. Dept., METU

Prof. Dr. Rıza Gürbüz _____
Metallurgical and Materials Eng. Dept., METU

Assist. Prof. Dr. Mert Efe _____
Metallurgical and Materials Eng. Dept., METU

Assist. Prof. Dr. Mehmet Yıldırım _____
Metallurgical and Materials Eng. Dept., KTUN

Date: June 13, 2019

I hereby declare that all information in this document has been obtained and presented in accordance with academic rules and ethical conduct. I also declare that, as required by these rules and conduct, I have fully cited and referenced all material and results that are not original to this work.

Name, Surname: Ali Fırat Dinler

Signature:

ABSTRACT

SYNTHESIS AND STRUCTURAL CHARACTERIZATION OF Co-Al BASED SUPERALLOYS

Dinler, Ali Fırat

M.S., Department of Metallurgical and Materials Engineering

Supervisor: Prof. Dr. Amdulla O. Mekhrabov

Co-Supervisor: Prof. Dr. M. Vedat Akdeniz

June 2019, 93 pages

Co-based superalloys are commonly used in static components such as stationary vanes because of their superior hot corrosion, oxidation, sulfidation resistance and phase stability at elevated temperatures. They possess relatively lower strength values due to limits in strengthening with solid solution and/or carbide precipitation that makes them unusable for blade and disk applications requiring higher strength values. However, Co-based superalloys with $L1_2$ ordered γ'-$Co_3(Al,W)$ microstructure has recently drawn attention as a suitable alloy structure which could be a substitute for the now-days extensively-used Ni-based superalloys.

In the first part of the investigation on the synthesis and structural characterization of Co-Al based superalloys; synthesis route, heat treatment regime and structural characterization of binary Co-Al alloys were presented. Co-rich side of Co-Al binary system was investigated by preparing 6 different alloy compositions (1.23, 8.40, 16.72, 19.50, 21.50 and 25 at. % Al), which were produced by arc melting technique. It has been found that relatively high Al content ($\geq$ 16.72 at. % Al) seemed to stabilize fcc-Co in as-cast state. For low Al containing alloys ($\geq$ 8.40 at. % Al) CoAl precipitation was not detected upon cooling from liquid state. It was shown that for these alloys fcc

to hcp transformation can occur via martensitic manner not requiring fast cooling rates. It is interesting to note that, microstructure and composition of as-cast and annealed (1300°C for 24 hours followed by furnace cooling) states of Co-Al binary alloys disagree and are not consistent with current equilibrium phase diagrams published in literature.

The superior properties of Co-based superalloys are originated from coherently distributed $L1_2$ type ordered $Co_3(Al,W)$-γ' precipitates within disordered γ matrix of Co-Al-W alloys. The phase stability of these ordered γ' precipitates in the extremely harsh service environment strongly depends on the ordering characteristics as well as coherency between γ and γ' phases. The aim of the second part of this study is to promote precipitation hardened Co-based superalloy microstructure for high-temperature applications. Therefore, the effects of tertiary alloying "W" element addition and heat treatments (including different aging times) on the solidification microstructures, structural stability and the mechanical properties of the Co-Al-W alloy systems with different Al & W content were presented. Through solutionizing and aging procedure until 256 h, γ/γ' microstructure was achieved. During the aging treatment, γ/γ' dual microstructure disturbed beneath the oxide layer and phases, namely Co_3W and Co_7W_6, that can degrade microstructural properties were formed. Structural investigations were performed by means of scanning electron microscopy (SEM), X-ray diffraction (XRD) and differential scanning calorimetry (DSC) techniques. Micro-hardness (Vickers) measurements were performed on as cast and heat-treated samples by using a Shimadzu Micro Hardness Tester.

Keywords: Co-Al binary, Co-based superalloys, $Co_3(Al,W)$ intermetallic, Microstructural evolution, Micro-hardness

ÖZ

Co-Al BAZLI SÜPERALAŞIMLARIN SENTEZİ VE YAPISAL KARAKTERİZASYONU

Dinler, Ali Fırat Dinler
Yüksek Lisans, Metalurji ve Malzeme Mühendisliği Bölümü
Tez Yöneticisi: Prof. Dr. Amdulla O. Mekhrabov
Ortak Tez Yöneticisi: Prof. Dr. M. Vedat Akdeniz

Haziran 2019, 93 sayfa

Co bazlı süperalaşımlar jet motorlarında yüksek sıcak korozyon, oksidasyon, sülfidasyon ve faz kararlılığından dolayı genel olarak hareket etmeyen, statik, parçalarda kullanılmaktadır. Bu alaşım grubu, düşük mukavemet değerlerinden dolayı (sadece katı çözelti ve karbür sertleştirmesi ile güçlendirildiği için) kanatçık ve disk gibi yüksek dayanım gerektiren uygulamalarda kullanılamamaktadır. Ancak, yakın zamanlarda miroyapısında $L1_2$ tipi düzenli γ'-Co_3(Al,W) çökeltilerine sahip alaşımlar, şimdilerde çok fazla kullanlan nikel bazlı süperalaşımlara alternatif olabileceğinden dolayı dikkat çekmiştir.

Yüksek sıcaklık uygulamaları için Co bazlı süperalaşımların tasarımı ve geliştirilmesi doğrultusunda, bu çalışmanın ilk kısmında Co-Al ikili sistemi çalışılmıştır. Kobaltça zengin kısımdan 6 farklı kompozisyon (% 1.23, 8.40, 16.72, 19.50, 21.50 and 25 at. Al) ark eritme metoduyla üretilmiştir. Görece yüksek Al içeren alaşımların (≥ % 16.72 at. Al) yüzey merkezli kübik yapıda olan Co katı çözeltisini döküm yapısında stabilize ettiği görülmüştür. Düşük Al içeren (≥% 8.40 at. Al) alaşımlarda ise sıvı fazdan soğuma sonrası CoAl yapısı görülmemiştir. Aynı zamanda yüzey merkezli kübik

yapının, hekzagonal sıkı paket yapısına fırında soğutma hızıyla bile martenzitik yolla dönüştüğü görülmüştür. Son olarak, dökülmüş ve ısıl işlem görmüş (1300 $^{\circ}$C'de 24 saat boyunca tavlanmış ve fırında soğutulmuş) mikroyapı ve onu oluşturan fazların bileşiminin mevcut olan Co-Al faz diyagramlarıyla uyuşmadığı tespit edilmiştir.

Kobalt bazlı süperalaşımların üstün özellikleri $L1_2$ tipi düzenli γ' çökeltilerinin düzensiz γ matriksinde düzenli bir şekilde dağılımıyla gerçekleşmektedir. Bu düzenli γ' çökeltilerinin son derece agresif servis koşulları altında faz kararlılığı düzenlenme karakteristiğine ve matrix ile çökeltilerin uyumluluğuna güçlü bir şekilde bağlıdır. Bu çalışmanın ikinci kısmının amacı yüksek sıcaklık uygulamaları için kobalt bazlı süperalaşımların tasarlanması ve geliştirilmesidir. Bu yüzden, üçüncül element ilavesi olan W'in farklı sürelerde yaşlandırma ısıl işleminin katılaşma mikroyapısı, yapısal kararlılık ve mekanik özelliklere farklı Al ve W oranlarıya etkisi incelenmiştir. Çözeltiye alma sonrası 256 saate kadar süren yaşlandırma işlemlerinde γ/γ' yapısı elde edilmiştir. Yaşlandırma işlemi sırasında oksijen ile temas eden dış yüzeyin altında ise γ/γ' yapısına ek olarak Co_3W ve Co_7W_6 gibi mekanik özellikleri düşürecek fazlar oluşmuştur. Yapısal araştırmalar taramalı electron mikroskopu (SEM), X-ray difraktometresi (XRD) ve diferansiyel taramalı kalorimetre (DSC) ile yapılmıştır. Mikrosertlik ölçümü (Vickers), alaşımlarım döküm ve ısıl işlemli hallerinde Shimadzu Micro Hardness Tester cihazıyla yapılmıştır.

Anahtar Kelimeler: Co-Al ikili sistemi, Kobalt bazlı süperalaşımlar, $Co_3(Al,W)$ metallerarası, Mikroyapısal evrim, Mikro-sertlik

To my dear parents

ACKNOWLEDGMENTS

I would like to state the inmost recognition to my both advisors, Prof. Dr. Amdulla O. Mekhrabov and Prof. Dr. M. Vedat Akdeniz for their everlasting concern, supervision, tolerance and aid in complex situations I faced during this thesis work. They were always open for sharing their guidance and intelligence. Also, they would let me lead this work on my own to give me the ability of being self-sufficient that I know it will pay off in my future life. Apart from my supervisors, I would like to thank my other committee members for their attitude and vast amount of genius that opened up new horizons in my mind.

In addition, a thank you to Asst. Prof. Dr. Mehmet Yıldırım of the Department of Metallurgical and Materials Engineering at Selçuk University. He guided me in the right way whenever I needed him. Additionally, I would like to thank all my lab mates in our lab, NOVALAB (Novel Alloys Design and Development Laboratory), especially to Iraz Begüm Demir whom she and I discussed on materials science for countless of hours. I also thank Efe Orhan with whom I started master's degree at the same time and shared good and bad times together during our thesis work. A deep gratitude goes to Nilüfer Özel, Serkan Yılmaz and Yusuf Yıldırım. They put up with me on numerous occasions without any single complain.

Finally, I cannot thank enough to my parents. They have always encouraged me to carry out and finish this thesis. This work would not be present if it were not for them.

TABLE OF CONTENTS

LIST OF TABLES

TABLES

LIST OF FIGURES

FIGURES

CHAPTER 1

INTRODUCTION

1.1. Aim and Motivation

Up to the present time, Ni-based superalloys have been broadly used in numerous high temperature applications such as hot sections of jet engines and land-based power generation gas turbines as rotor (moving) or stator (stationary) parts requiring high temperature (T≥500 °C) mechanical and environmental resistance. On the contrary, conventional Co-based superalloys have been confined to relatively low mechanical strength requiring stationary components due to non-existence of main strengthening mechanism that would be Co_3Al. The discovery of the precipitation of $L1_2$ ordered γ'-$Co_3(Al,W)$ phase in the ternary system of Co-Al-W created a great wave of research flux in superalloy development area [1]. Existence of strengthening precipitations bound to improve tensile, fatigue and creep properties of Co-based superalloys. Because of the comparably slight lattice mismatch between the γ' and γ phases, emerging γ' phase takes up a cuboidal morphology in the disordered γ-Co solid solution from which it precipitates. Resulting microstructure becomes γ/γ' and some carbides if carbon is present, which essentially the same microstructure as precipitation hardened Ni-based superalloys. Novel γ/γ' Co-based superalloys have been appealing enormous attraction to engineers since they can upgrade theoretical limitations in Ni-based superalloys.

For jet engines, fuel efficiency is directly proportional to operation temperatures. Yet the solvus temperatures of γ' precipitates in Ni-based superalloys have almost maxed out their limit which means they are close to their incipient melting temperatures. On the other hand, precipitation hardened Co-based superalloys possess greater upper limit, because their melting temperatures are 50 - 150 °C higher than those of Ni-based superalloys. The fundamental reasoning behind this phenomenon is that pure Co has melting temperature 40 °C higher than that of Ni. This, in turn, means Co-based superalloys would work at lower homologous temperatures leading to better creep lives.

In this work, it is aimed to design and develop Co-based superalloys for high-temperature applications by first examining Co-Al binary system and then by investigation γ' precipitation after W addition by means of SEM, DSC, XRD and microhardness.

1.2. Contribution

In literature, there are limited knowledge on Co-rich side of Co-Al binary system. There are dashed lines on Co rich side meaning that there are not enough data to plot solid lines. In this work, 6 different compositions of Co-Al binary alloy system were determined to investigate microstructural characteristics of Co rich part of the system. Annealing treatment was carried out after casting to ensure equilibrium state is reached.

As for ternary alloy (Co-Al-W), two different compositions were cast. After investigation of as-cast state of these alloy, aging procedure was performed according to the DSC results of as-cast structure. γ' precipitation was observed for both ternary compositions after aging treatment.

CHAPTER 2

THEORY

2.1. Co-Al Binary System

Among Co-based binary commercial alloys, Co-Al binary stands out as one of the most essential system. It can be used as hard magnets [2], shape memory alloy [3-7] and a base alloy system for high-temperature applications [1]. In literature, there have been some both experimental [8, 9] and calculated phase diagrams [10-13] published yet they are all inconsistent with each other and there are dashed lines in Co rich side implying that there are not enough data to plot solid lines.

The Co-Al diagram was reported to be first investigated by Guillet [14, 15] and then few years later Gwyer [16] reported a full phase diagram after examination of microstructural characteristics and time vs. temperature cooling plots for as much as 30 different alloy compositions. As a result of this work, three intermetallics were described and labelled as Co_3Al_{13}, Co_2Al_5 and CoAl in terms of their compositions. In addition, any hcp and fcc-Co phase differentiation was not defined. Hansen et al. [17] stated in his work that eutectic composition lies at 19.5 % at. Al however this proposal was revised by Stout et al.[18]. In his study, the eutectic composition was given as 18.7% at. Al. Also, in 1985 Wall et al. [19] found eutectic composition very close to the one suggested by Stout.

In 1993, Köster [20] published a paper where binary Co-Al and ternary Co-Al-Fe alloys were examined. Eutectic point was given as 19.5 % at. Al for binary alloy and again there was no mentioning polymorphic transition from fcc to hcp-Co. Dupin and Ansara stated in their work [21] that two phase field of fcc-Co+CoAl needs extensive annealing time to achieve thermodynamic equilibrium because of considerable variation in solubility. In 1989, McAlister had published the most extensive phase diagram [8] covering all the past work on Co-Al binary system. The published diagram is given in Figure 2-1. It is clear from the diagram that there are too many dashed lines which point there was still lack of data for drawing solid lines instead of dashed ones.

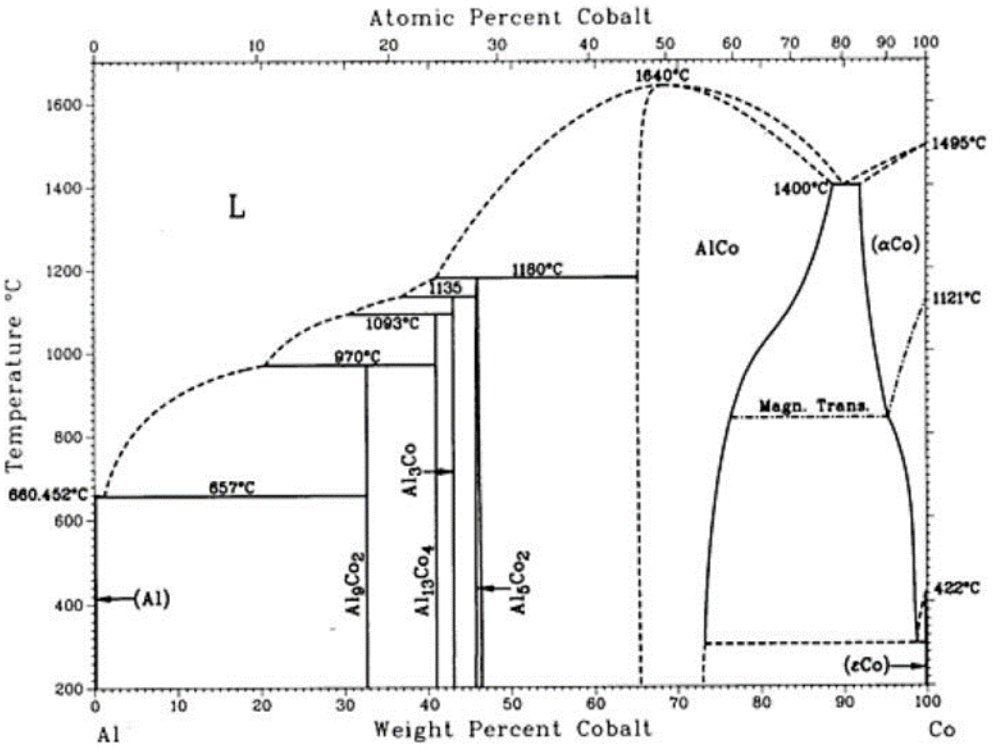

Figure 2-1 Co-Al phase diagram published by McAlister [8].

After publishing of the binary phase diagram by McAlister in 1989, the most comprehensive work on Co-rich side of Co-Al binary system was done by Kimura et al. [22]. They prepared series of Co-Al binary alloys ranging from 40 at. % Co to 98 at. % Co by using arc melting method. Alloys were then annealed at 1000 °C for 7 days or 1150 °C for 48 hours. It was claimed that 72 & 76 at. % Co alloy had Co precipitation at the grain boundaries of CoAl phase and 80 at. % Co alloy had eutectic structure. Optical micrographs were given in Figure 2-2.

Figure 2-2 Annealed microstructures of (a) 72 at. %Co, (b) 76 at. %Co and (c) 80 at. %Co [22].

Bright phase is hcp-Co phase as it can be understood from its TEM analysis (Figure 2-3) where stacking faults exist in blocky Co meaning that fcc-hcp transformation occurred during cooling from annealing temperature. However, there was no report on fcc-Co to hcp-Co transformation temperature that is expected to happen at 300 °C even though DTA measurements were run on annealed alloys.

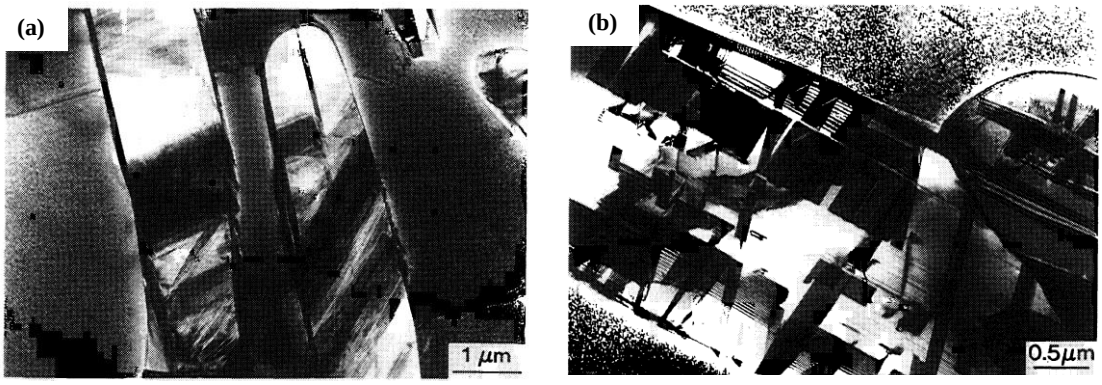

Figure 2-3 TEM micrographs of 76 at % Co alloy after annealed at 1150 °C for 48 hours. (a) Co phase in CoAl matrix, (b) stacking faults in Co phase indicating fcc-hcp transformation [22].

Most recently, a research done by Kazantseva [23] on 9 at. % Al alloy found out that composition of phases and microstructure do not agree with the equilibrium phase diagrams currently available. They also stated that fcc to hcp transformation may occur via martensitic manner even in furnace cooled specimens that are annealed at 1250 °C after casting.

In literature, an interesting phenomenon called discontinuous precipitation was observed in Ni-Al [24], Co-W [25], Co-Mo [26, 27], Ni-In [28, 29], Ni-Co-Al [30, 31] and even in Ni-based superalloys[32]. In addition to these systems, discontinuous precipitation also was found in Co-Al system [33, 34]. It is a solid-state reaction in which a solid solution that is in supersaturated condition dissolves into a solute-depleted matrix and solute-rich precipitates across a migrating grain boundary or reaction front resulting in a two-phase lamellar product. Alternative plates of the Co-rich solid solution and the intermetallic compound nucleate at high-angle grain boundary [25, 35]. An example of this structure is given in Figure 2-4 [34].

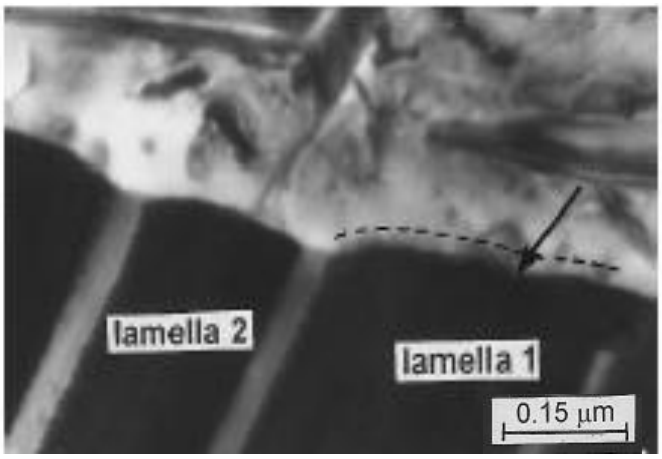

Figure 2-4 TEM image illustrating lamellar structure of discontinuous precipitation in 13% at. Al alloy after aged at 800K for 2 h and subsequent 950K for 20 min second aging [34].

In the supercooled β phase, extremely fine ϵ plates are known to precipitate at relatively high temperatures in the α-Co+β-CoAl two phase region of the Co-Al phase diagram and induce a great coercivity [36, 37]. In addition, both experimental[38-40] and thermodynamic [41] examinations claim that in the same α-Co+β-CoAl region of the Co-Al system metastable phase separation of A2-Co and B2-CoAl phases takes place. Kamiya et al.[40] empirically confirmed the compositions of metastable region of α-Co+β-CoAl of Co–Al binary alloy by extrapolating the equilibrium data of Co-Al-Fe. The experimental results are superimposed on Co-Al binary diagram in Figure 2-5 [42]. Niitsu et al. assert that the presence of this metastable region is the reason why Co-Al binary system does not form a stable $L1_2$-Co_3Al.

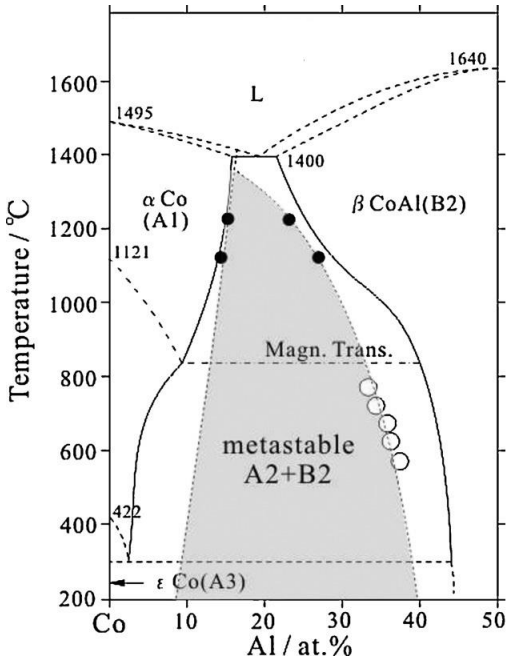

Figure 2-5 Co-Al phase diagram showing metastable regions [42].

In Co>50 at. % part of Co-Al system, phases present are (1) fcc-Co solid solution which can be paramagnetic or ferromagnetic depending on composition and temperature. Its maximum equilibrium Al content is about 16 at. % [17] , however metastable fcc-Co can hold up to 17 at. % Al when quenched from liquid state [43] (2) hcp-Co that has virtually no solubility of Al [44, 45]. Metastable phases of hcp-Co are also reported in literature. They are reported to form when single crystal fcc-Co solid solution having 4-16 at. % Al is heated in the vicinity of 1200 °C, quenched and subsequently aged in the range 400-800 °C for some time and immediately quenched down to -200 °C [46]; (3) B2-CoAl that can also exist as off-stoichiometric towards Co end of the diagram. Due to having relatively low density, exceptional oxidation resistance and superior yield strength,

this B2 ordered intermetallic has once been recognized as an enticing material for a broad scope of engineering operations[47-49]. However, it's extremely brittleness makes it unable to be formed into a desired shape [50]. Crystal structures contained in Co rich side of Co-Al binary system is tabulated in Table 2-1.

Table 2-1 Summary of phases in Co-rich side of Co-Al binary

Phase	**Composition % at. Al**	**Crystal Structure**
Stable Phases		
CoAl	~48-78.5	B2
ϵ-Co	0	hcp
α-Co	84	fcc
Metastable Phases		
α^1	4-11	hcp
α^2	12-14	hcp
α^3	14-16	hcp
α^4	12-14	hcp

To sum up the findings about Co rich side of Co-Al binary system, the position of Co-Al eutectic (in Co rich side) is ambiguous in literature. Besides there is too little information regarding fcc-Co to hcp-Co transformation that is supposed to occur at 300 °C when Co is alloyed with Al.

2.2. Superalloys Overview

A specific family of alloys shows outstanding capability to sustain their mechanical properties such as yield strength, creep etc. at temperatures $T \geq 0.5T_m$. These alloys are called superalloys. They suit themselves in many high temperature & high stress applications such as jet engines and power plants. As for these operations, the performance of the operating system is restrained by the service conditions that may be countered by the alloys used. For instance, power output and efficiency of a natural gas plant depends directly to mechanical capabilities of the superalloys used in its harshest sections.

There are some required performance characteristics that superalloys need to meet. First of which is to resist stresses in service conditions close to material's melting point. There is a relative temperature designation called homologous temperature (T_H). It is defined as the ratio of the temperature of a material to its melting point in Kelvin scale. So, the alloy should be capable of operating at least 0.6 T_H. Secondly, the materials should have excellent long-term mechanical properties such as creep. Alloys possessing low creep accumulation rates ($\dot{\varepsilon}_{creep}$) are preferred for high temperature applications. Along with long term mechanical properties, short term properties like tensile strength or fracture toughness are of importance and should be sustained for long periods of time. Final consideration is resistance to environmental conditions. In natural gas plants or coal-fired plants sulphur-oxides create a highly corrosive atmosphere for crystalline metallic alloys. Superalloys should have enough environmental resistance to this kind of rough environments. In many cases, these alloys are bond coated with MCrAlY (M= Ni and/or Co) type of layer and having a final thermal barrier coating (TBC), usually being yttria-stabilized zirconia (YSZ) at the top to maximize the protection [51] .

Superalloys are classified in accordance with the major element in the alloy. There are 3 different types of superalloys; namely Ni-Fe, Ni and Co based superalloys.

The common properties of these three alloy groups is that they are all composed of face-centered cubic (fcc) matrix meaning that they are inherently tough and ductile. Out of these three elements only Ni has fcc structure at room temperature while other two need alloying elements to stabilize their high-temperature phase, fcc, at ambient temperatures.

2.2.1. Nickel-Iron Based Superalloys

These alloys are distinguished by their great ductility and toughness and are employed typically in applications in which these properties are essential, for example turbine rotors or discs. Therefore, Ni-Fe alloys are used solely in the wrought form, since this manufacturing technique presents an extensive diversity of mechanisms for adjusting morphology and grain size. Along with their great toughness, one more benefit of Ni-Fe based superalloys is that they cost less because of the considerable sum of iron added[52].

These alloys are developed from austenitic stainless steels. The austenitic matrix (γ) is established by Fe and Ni where Ni is required to stabilize the fcc phase as it is shown in Figure 2-6 [53]. Second main alloying element, which is Cr, partition mainly to the γ matrix for solid-solution hardening and corrosion resistance. There are three branches of Ni-Fe based superalloys. The first of which is the precipitation hardened superalloys, where the main strengthening phase is $L1_2$ ordered γ'-$Ni_3(Al,Ti)$ and/or DO_{22} ordered γ''-Ni_3Nb precipitates that are formed in the disordered fcc γ matrix as in the case for IN-718. The second one is called low coefficient of thermal expansion (CTE) type and utilized for applications where low thermal expansion is required. The third one is the modified stainless steels, chiefly strengthened by solid-solution hardening and carbide phases as in the case for traditional Co-based superalloys.

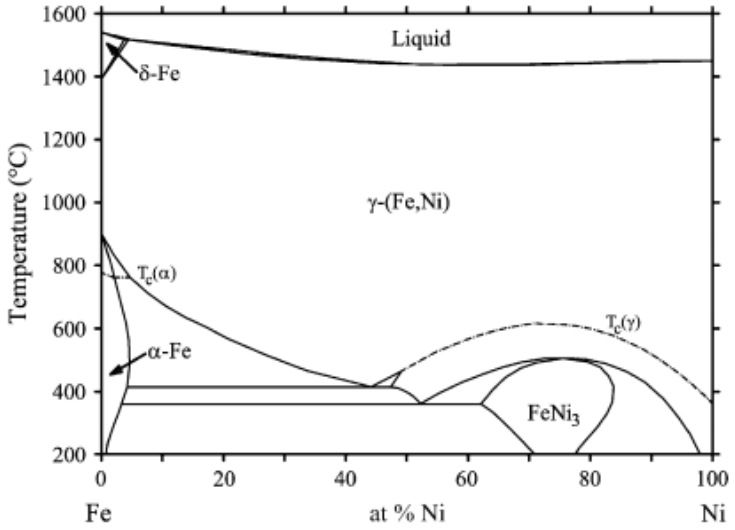

Figure 2-6 Fe-Ni binary phase diagram [53].

2.2.2. Nickel-Based Superalloys

Ni-based superalloys are employed in a variety of gas turbine components due to their excellent high-temperature properties. These materials have, in general, high strength at elevated temperature, high creep resistance, high fatigue resistance and satisfactory corrosion resistance. They can work up to $0.9T_{m.}$ They owe their excellent mechanical properties to their so called γ/γ' microstructure. The gamma matrix (γ) is disordered Ni-fcc phase and γ' is $L1_2$-ordered (Ni_3Al) intermetallic phase. Ni-based superalloys are based on the Ni-Al binary system (Figure 2-7 [54]).

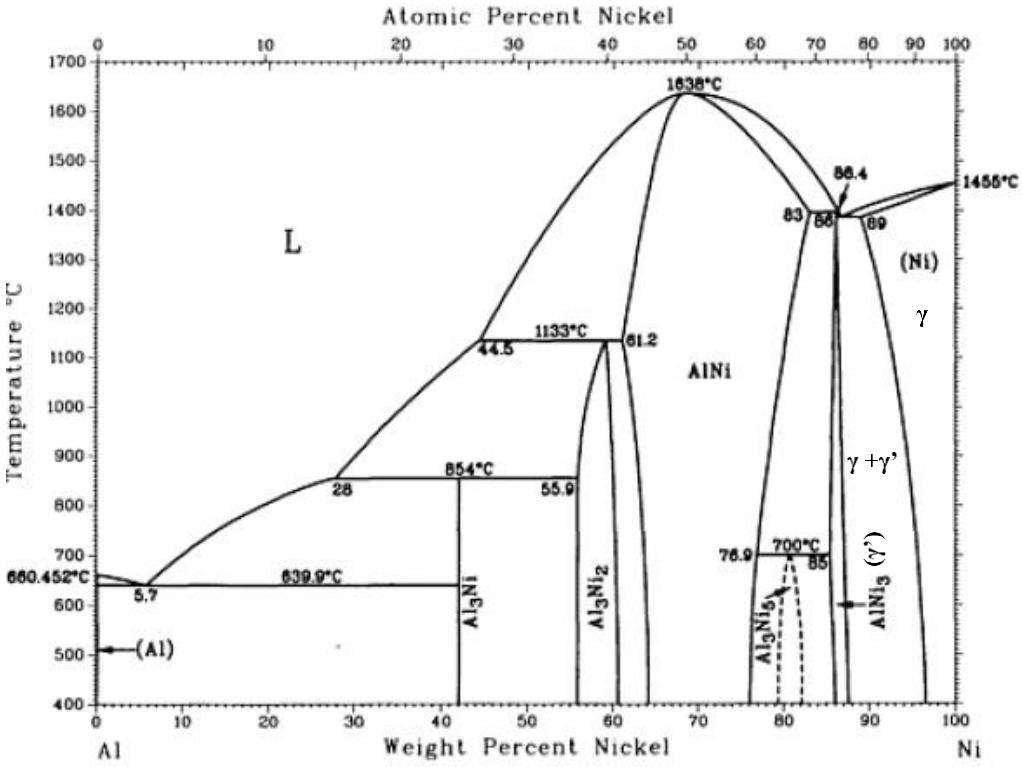

Figure 2-7 Ni-Al phase diagram [54]

Solutionizing this binary system generates a supersaturated fcc-γ disordered solid-solution and subsequent aging produces an ordered $L1_2$-ordered Ni_3Al precipitate in a composition range of γ+γ' as shown in Figure 2-7 [54]. The γ' precipitates possess the Cu_3Au prototype where the Ni atoms reside at the cubic faces and Al atoms sit at the cubic corners (Figure 2-8) [55]. These precipitates are coherent with the γ matrix and retain a minor lattice parameter misfit (δ) that leads to high phase stability and hence small coarsening rates at higher temperatures [56-60].

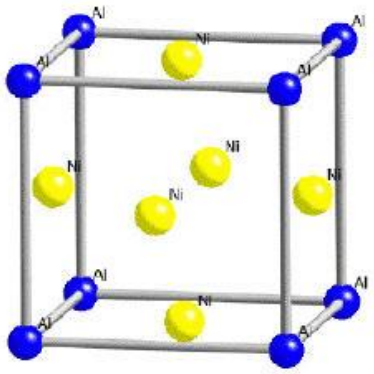

Figure 2-8 Superlattice structure of $L1_2$ ordered Ni_3Al.

Traditional Ni-based superalloys have developed significantly with regards to both processing and composition from the Ni-Al binary system. Conventional Ni-based superalloys generally comprise between 8 to 12 different alloying elements. Cr is added to almost all Ni-based superalloys to improve high-temperature oxidation resistance [61]. Refractory elements namely Mo, W, Re, Ru partition to the γ matrix to increase mechanical properties such as creep via solid-solution strengthening mechanism and reduce coarsening rate yet they may form Topologically Closed Packed (TCP) phases that are detrimental to the mechanical properties when added in excess amounts [62-64]. Tantalum and Titanium work as γ' stabilizers [65, 66]. To enhance grain boundary strength, minor element additions of B, Zr, and C are introduced to polycrystalline alloys by segregating to the grain boundary which form carbide (MC, $M_{23}C_6$, M_6C) or boride (M_5B_3) grain boundary precipitates [67, 68]. Nevertheless, these grain boundary elements have been rendered obsolete in single crystal alloys where GB strengthening is not required since there is not any of them.

Together with the progress in superalloy chemistry, developments in processing have been critical to the improvement of state-of-the-art Ni-based superalloy discs and airfoils as

shown in Figure 2-9 [51]. In the 1940's, the primitive Ni-based superalloys were manufactured in wrought state in which the alloys were in polycrystalline from and restricted to service temperatures under 900 °C. In the 1950's, cast superalloys which can be produced into complicated turbine blade shapes far easier than wrought alloys were introduced.

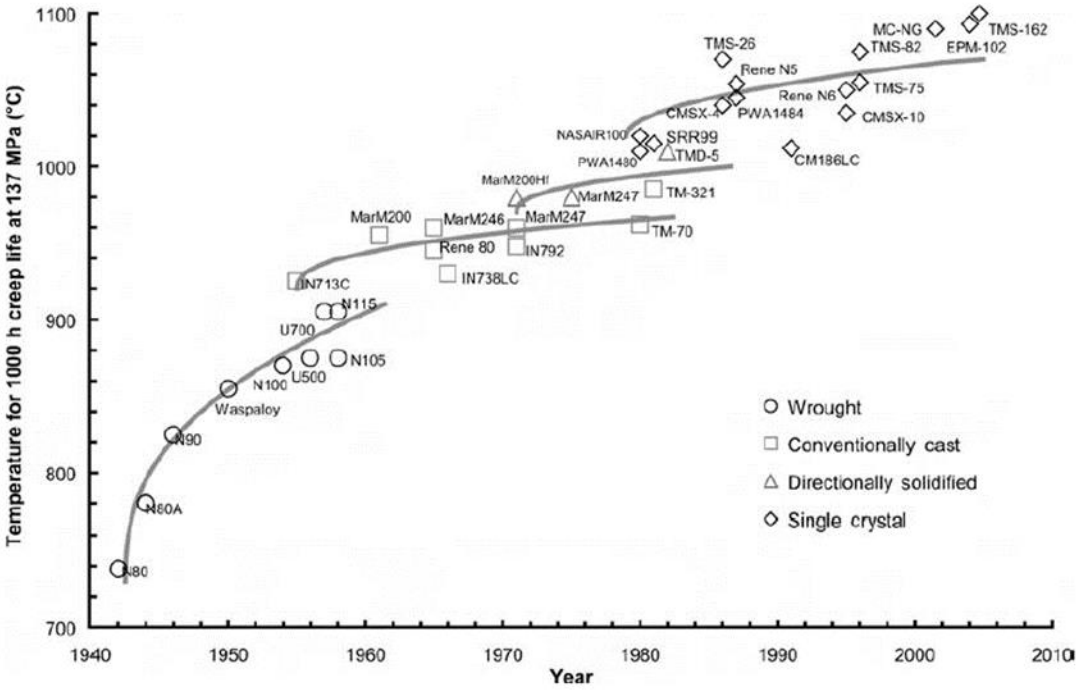

Figure 2-9 Superalloys developed throughout years [51].

Directionally solidification (DS) by which the superalloys are fabricated to be composed of coarse grains which is aligned along the airfoil dimension enhanced rupture properties especially at elevated temperatures. Lastly, the introduction of single crystal airfoils where grain boundaries are completely removed from the alloy itself have made their uses to be

able to work at even higher service temperatures than any other production methods (Figure 2-10 [51]).

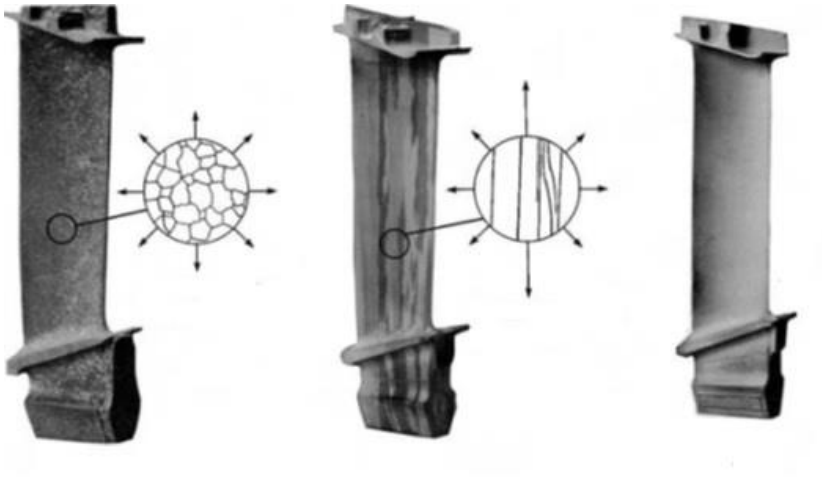

Figure 2-10 Blades having polycrystalline, DS and SX structure [51].

2.2.3. Strengthening Mechanisms

There are 4 main strengthening mechanism in Ni-based superalloys. These are namely; solid solution, precipitation, coherency and grain boundary strengthening. There are also other mechanisms that contribute to mechanical properties such as stacking fault, modulus and chemical strengthening but their effect is minimal because of comparable properties of γ' and γ phases [69-71].

2.2.3.1. Solid Solution Hardening

Ni-based superalloys consist of numerous elemental additions that may rest on the lattice sites of the γ' and γ structures. The lattice of parent γ matrix gets distorted in the vicinity of solute atom due to difference in atomic radius of Ni and solute atom. The resultant strain field reacts elastically with that of a dislocation, by that hindering dislocation movement and eventually developing the strength with respect to pure Ni. These interactions come from misfit in atomic size and elastic modulus [72]. The elastic modulus misfit originates from the existence soft and hard fields in the matrix that occurs due to difference in stiffness of solute atoms and parent phase. The solid solution strengthening is generally considered to be in the parent γ matrix phase [73, 74], for that it is hardly examined in the γ' phase because of its ordered nature [75, 76]. Solid solutions also display short range order to some degree. The energy necessary to shear a crystal with short range order results in increase in yield strength. It has been shown that Ni-Cr binary exhibits short range order in the range of 20 to 25 wt. %. This compositional range is matched in some Ni-based superalloys such as Hastelloy-X and Inconel 625 [77].

2.2.3.2. Precipitation Hardening

It is commonly postulated that the strength of superalloys is directly proportional to the volume fraction of γ' precipitates. As it is well known for a fact that in Ni-based superalloys, plastic deformation chiefly takes place with the movement of a $\alpha/2<110>\gamma$ dislocation type (here `a` represents the lattice constant in the disordered fcc matrix phase). But, the $L1_2$ ordered nature of the γ' puts the atoms into high energy state creating anti phase boundary energy (APBE) when dislocations move with the aforementioned mechanism. For that reason, the dislocations must move in pairs to bring back the original γ' structure when ordered precipitates exist in the system, [71].

γ’ precipitate size determines the mode of deformation. If precipitates are relatively small deformation takes place by pairs of α/2<110>γ cutting through the particles, with an APB between them. For a pair of dislocation, the leading one creates APB whereas trailing one eliminates it. Small precipitates are cut by dislocations rather than being bowed, each dislocation in the pair is situated in a different precipitate (weak pair coupling) .On the contrary, in relatively larger particles strong pair coupling occurs where each dislocation in the pair is located in the same precipitate due to having larger APBE [76].

In the case of larger precipitates, deformation occurs via Orowan looping [78, 79]. It is frequently accepted that the maximum strength of superalloys develops when the precipitate sizes match to the change between strong and weak pair coupling, at a constant temperature [73]. This means that bimodal size distribution is the optimum condition for alloy strength [80].

2.2.3.3. Coherency hardening

The mismatch in lattice constant of the matrix and particles is another factor that contributes to strength of an alloy by hindering dislocation motion. Evidently, lattice misfit (δ) between the γ’ and γ phases is the main parameter in determining the contribution of coherency strengthening. The formula of the lattice misfit (δ) is given below [51]. Note that $\alpha_{\gamma'}$ is the lattice parameter of precipitate and α_{γ} is the lattice parameter of the matrix

$$\delta = \frac{2(\alpha_{\gamma'} - \alpha_{\gamma})}{\alpha_{\gamma'} + \alpha_{\gamma}}$$

One important point in calculating the lattice misfit is that there is distinction in constrained and unconstrained lattice parameters. The constrained lattice constant is calculated in the γ/γ' in which the lattice constants of both phases become closer values

over the matrix/precipitate interface in order to preserve coherency. For example, in negatively misfitting systems, the lattice constant of the γ' phase is smaller than that of the γ and hence forced to increase. As for unconstrained case, lattice constants of both phases measured in their single-phase material meaning that they are unaffected by a neighboring phase. Contrary to the constrained lattice constant, this is the basic parameter that does not rely on the precipitate morphology, size or interface orientation with respect to the matrix. Most of the existing commercial Ni-based alloys have been constructed in such a way that the negative misfit between the γ and γ phases is present. In this case, the matrix phase is under a compressive load whereas precipitates are under tensile load. As a result, the driving force for dislocation motion in the softer γ channels decreases and consequently the alloy strength increases. The misfit is mainly arranged as ($\sim 10^{-3}$) to reduce precipitate coarsening at high temperatures [81].

2.2.3.4. Grain boundary strengthening

As it is one of the most fundamental mechanism in all alloy types, the existence of grain boundaries increases the yield strength of polycrystalline alloys at relatively low temperatures. The dislocations motion is disrupted by the presence of grain boundaries, so bigger loads are needed to plastically deform an alloy [76].

2.2.4. Cobalt-Based Superalloys

2.2.4.1. Traditional Cobalt-Based Superalloys

Traditional Co-based superalloys emerged in the early 1900's with the beginning of investigation Co-Cr and Co-Cr-W alloys. As a result, trademark Stellite alloys under Haynes Company evolved into valuable industrial materials for saw teeth, hardfacing and acid-resistant machine parts. Years later, cast Co-Cr-Mo ternary alloy called Vitallium arose for dental purposes and its sister HS-21 suited itself in gas turbine or turbocharger operations in 1940s. However newer version of this alloy called X-40 (Co-Ni-Cr-W) displaced HS-21 in turbine or turbocharger applications. In addition, Co-Ni-Cr wrought alloy was widely employed in rotor and stator parts of jet engines.

With the advancement of casting techniques (electro slag refining, double or triple melting) in γ' containing Ni-based superalloys in 1950s eclipsed the effectivity of Co-based superalloys because of non-existent Co_3Al precipitation. This Ni-based superalloy superiority took a huge chunk out of Co-based alloys in high temperature applications. Furthermore, seasonal price and accessibility problems in Co mine damaged its potential use even further. However; they are still in use over Ni-based superalloys due to following reasons:

Co-based superalloys have higher melting point thus having flatter creep rupture curves which make them available to be used higher temperatures than Ni-Fe or Ni-based alloys. Since Co-based superalloys have more chromium than that of Ni alloys, their hot corrosion resistance is superior to that of Ni alloys. Overall better TMF (thermo-mechanical fatigue) resistance and weldability. The chemical composition of traditional Co-based superalloys is similar to those of austenitic stainless steels and the role of alloying elements are almost same. Table 2-2 Chemical compositions of Haynes 188 and 304 stainless steel in at. %. (Table 2-2) [77].

Table 2-2 Chemical compositions of Haynes 188 and 304 stainless steel in at. %.

	Co	**Ni**	**Cr**	**W**	**Fe**	**Mn**
Haynes 188	Bal.	22	22	14	3	1.25
304 SS	-	8	18	0.3	Bal.	1.8

Particularly, the main alloying element is Cr which is added 20-30 wt. % to give oxidation and hot corrosion resistance along with minor solid solution strengthening. One should be wary of excess amount of chromium additions as it forms very brittle σ phase figure.

Carbide strengthening also plays an important role where Cr forms different carbides, $Cr_{23}C_6$ type being the most prominent one (Figure 2-11 [82]). Its effect is seen the most profound in creep rupture strength. In addition, tensile strength is directly proportional whereas ductility is inversely proportional to carbon content in the range of 0.3 to 0.6 wt. % carbon. They are also critical in grain size controlling during processing, heat treatment and following service life.

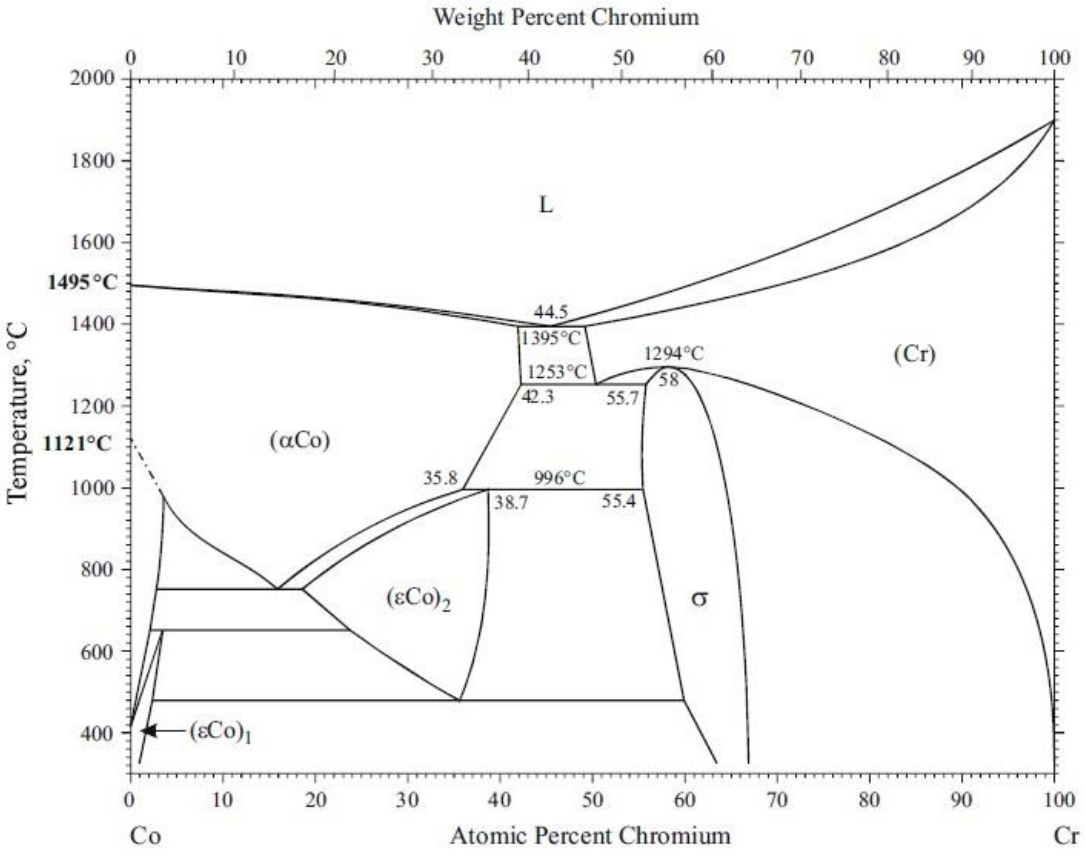

Figure 2-11 Co-Cr phase diagram *[82]*.

Refractory elements such as Mo and W are used primarily as solid solution strengthening for cast and wrought alloys. Other elements Ta, Nb, Zr and Hf are commonly employed as MC type carbide formers. It should be noted that excessive amount of refractory element additions can cause deleterious TCP or Laves phases.

In order to improve the stability of austenitic fcc-Co matrix, element additions up to 20 wt. % Fe or Ni are employed to avoid any possible fcc to hcp transformation that could happen at lower temperatures which in turn would make the alloy unstable. These additions also make the Co alloys more workable.

Si and Mn elements are used to improve castability (decrease viscosity), sulfur control and deoxidizing. Al is beneficial in hot corrosion and oxidation resistance (Table 2-3).

Table 2-3 Effect of various element additions on Co-based superalloys [77] .

	Cr	**C**	**W,Mo**	**Ni,Fe**	**Ti,Zr,Ta,Nb**
Primary Function	Surface protection	Carbide former	Solid solution strengthening	fcc stabilizer	Carbide former
Possible Disadvantages	TCP former	Lowers ductility	TCP former	Lower corrosion resistance	Lowers surface stability

Typical microstructure of traditional Co-based superalloy is shown in Figure 2-12.

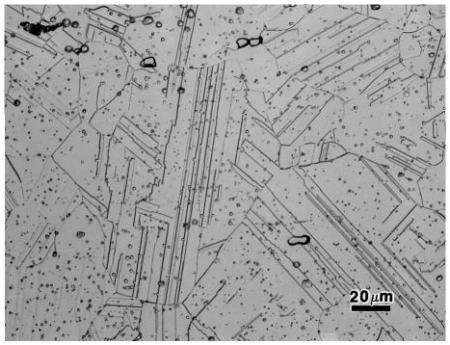

Figure 2-12 Microstructure of Haynes 188 alloy [83].

2.2.4.2. Modern Cobalt-Based Superalloys

It is a well-known fact that unlike Ni-Al binary system where $L1_2$ ordered γ' can precipitate, Co-Al [11] and Co-W [84] binary alloy systems cannot form a stable $L1_2$-γ' precipitates. However, the discovery of precipitating $L1_2$ ordered γ' precipitates in Co-Al-W ternary alloy system by Sato et al. created a new wave of research area [1]. According to the phase diagrams drawn by using Thermo-Calc TCNI8 (Figure 2-13) database it may be possible to obtain γ/γ' microstructure (shown as fcc_L12+fcc_L12#2 in phase diagram) in Co-Al-W ternary system at 900 °C. Also, the solvus temperature of Co-based superalloys is comparable to that of Ni-based superalloys.

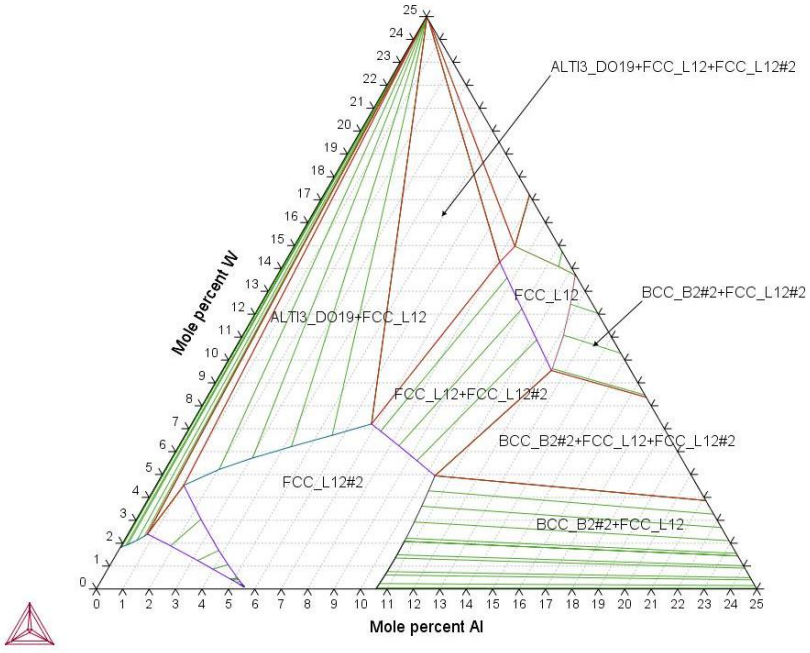

Figure 2-13 Co-Al-W phase diagram drawn by using Thermo-Calc TCNI8 database.

2.2.5. Phase Stability of $L1_2$-γ' Precipitates in Co-Al-W System

Sato et al. claimed that $L1_2$-γ' precipitates they found in their ternary alloys to be stable at 900 °C whereas unstable at 1000 °C. Xue et al.[85] examined the stability of $L1_2$-γ' precipitates that are aged at 900 °C for up to 1000 hours in Co-Al-W system. It was shown by means of SEM imaging and XRD method that γ/γ' is stable up to 1000 hours.

However it was later proposed by Kobayashi et al. [86] that $L1_2$ ordered $Co_3(Al,W)$ phase was also metastable at 900 °C. They employed a diffusion couple of Co-W (at. 15% W) and Co-Al (at. 27% Al) and quantified the diffusional path across the adjoined surface. In this study, it was discovered that $L1_2$-γ' phase was decomposed into Co_3W and CoAl phases as a result of the processing time up to 2000 hours at 900 °C. Another study on this subject conducted by Tsukamoto et al. [87] concluded that area fraction of γ' precipitates in Co-Al-W system is inversely proportional with the annealing time from 100 hours to 2000 hours at 900 °C. It also was stated that Co_3W and CoAl phases take up the place of diminishing precipitates. However, it should be kept in mind that proposed concentration is out of γ/γ' two phase region according to the study which includes thermodynamic evaluation of the Co-Al-W ternary system by preparing different alloys in and out of the γ/γ' two phase region at 900 °C [88]. Subsequent aging at 900 °C for up to 8000 hours reveals that all specimens exhibit CoAl, Co_3W, and/or Co_7W_6 phases depending on the composition and volume fraction of γ' precipitates declined proportional to time. Also, various efforts were made to produce a single-phase $L1_2$-γ' $Co_3(Al, W)$ microstructure as that can be obtained in the Ni-Al system. However, those attempts have often failed due to the presence of Co_3W or CoAl phases in the system [89-91].

2.2.5.1. Alloying Effect on the Stability of the γ'-Co_3(Al, W) Phase

The stability of $L1_2$-γ' Co_3(Al,W) has been shown to be improved by γ' stabilizers such as Ti, Ta, and Hf [92-94]. Measuring increase or decrease in the γ' solvus temperature is the most effective way to evaluate its stability when quaternary element is added. γ' solvus temperature of Co-Al-W ternary system is not as high as that of Ni-based superalloys. To give an example, in Co-9Al-11W ternary system where 79% volume fraction of γ' is obtained by aging at 900 °C, γ' solvus temperature can only reach up to 1030 °C. Table 2-4 shows the change in the γ' solvus temperature as a result of quaternary elemental additions in at. % [95-101]. Not that quaternary element additions were made in expense of Co in the ternary system. Expectedly, tantalum turns out to be most effective element in stabilizing γ', other effective ones are Ti, Nb, W, and Hf in descending order. On the other hand, Fe, Cr and Mn elements impart stability of γ' as they partition to the γ matrix [95].

Table 2-4 Change in the γ' solvus temperature versus quaternary elemental additions in at. %.

	Ti	**V**	**Cr**	**Mn**	**Fe**	**Ni**
γ' solvus change per addition of element in at. %	29	9	-2	-10	-5	**2**

	Zr	**Nb**	**Mo**	**Ru**
γ' solvus change per addition of element in at. %	5	28	5	**-5**

	Hf	**Ta**	**W**	**Re**	**Ir**
γ' solvus change per addition of element in at. %	15	45	18	-9	**1**

2.2.5.2. Mechanical Behavior Of The γ' -$Co_3(Al,W)$

Figure 2-14 illustrates variation of yield strength with temperature of ternary Co-Al-W alloy, a solid-solution-strengthened commercial Co-based alloy (such as Haynes188) and a commercial Ni-based superalloy. The yield strength of the Ni-based alloy is superior to Co-based counterparts due to having both precipitation and solid solution strengthening mechanism whereas commercial Co alloy lacks precipitation.

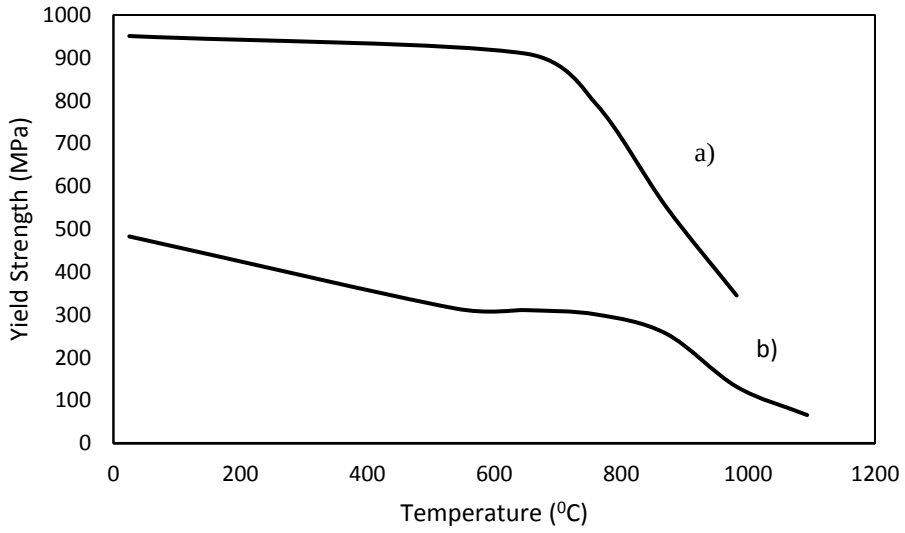

Figure 2-14 Temperature dependence of yield strength of a) Inconel 738 and b) Haynes 188 alloys.

Yield strength anomaly seen in γ' hardened Ni alloys is also seen in precipitation hardened Co alloys at around 800 °C. Increasing temperature further from this point lowers the yield strength of alloy due to excessive coarsening and eventual dissolution of precipitates. At moderate temperatures, slip on <110>{111} is the dominant deformation mechanism as the lattice is face centered cubic. <110>{001} slip system gets thermally activated by

raising temperature and TEM analysis showed that cross-slip of 1/2<110> dislocations to the cube {001} from the octahedral {111} plane in the γ' precipitates is analogues to γ/γ' Ni-based alloys [102].

Creep strength is always one of the most important feature of high temperature alloys. Creep and rupture properties have been studied in precipitation strengthened Co alloys. Study shows that Co-9Al-(8–9)W-2Ta-2X (X = Nb, Mo, Ir, V, Cr, or Si) exhibit relatively inferior creep properties when compared to Ni-based superalloys because of large scale strain aggregation at grain boundaries . Boron doping can boost creep properties by enhancing the resistance of grain boundaries to strain aggregation [103].

An intriguing array of deformation mechanisms take place in the course of creep deformation of modern Co-based superalloys. In the primary stage of creep, deformation takes place broadly by glide of a/2<110> dislocations over the austenitic γ matrix, with a greater initial dislocation amount in the vertical channels because of the stress state activated by γ' precipitates that have positive misfit with the matrix. Similar to Ni-based superalloys, Co-based superalloys are also subjected to precipitate rafting, with significant difference that the rafts largely grow with their longitudinal axis parallel to the applied force because of positively misfitting of matrix and precipitate. The lowest creep resistance is observed in almost fully coherent precipitate/matrix alloys, and as explained in chapter X the strongest ones are negatively misfitting systems.

CHAPTER 3

EXPERIMENTAL PROCEDURE

3.1. Raw Materials

Alloys were prepared by using nearly pure elements produced by Alfa Aesar. The purity levels (wt. %) of Co, Al, and W used in this study are 99.90, 99.90, and 99.95 respectively.

3.2. Production of Alloys with Arc Melting

Both binary and ternary alloys were produced by employing arc melting furnace (Figure 2-15). Before melting procedure, the component elements of the alloys were cut from their respective pure blocks and were weighed according to desired composition by using precision weighing balance. The melting of solid mixtures was done on a water-cooled copper tray having a non-consumable tungsten electrode on top of it. To prevent oxidation of alloys during melting, the camber was flushed with argon 3 times and vacuum level was reduced to 10^{-5}mbar with the help of rotary and diffusion pump. A Zr ball was placed in the chamber to act as oxygen getter. Alloys were melted 3 times to make sure homogeneity throughout the solidified alloys. The produced alloys were re-weighed to measure possible Al losses during melting.

Figure 2-15 Arc melting device.

3.3. Heat Treatment

As-cast binary alloys were heat treated to eliminate any inhomogeneities, segregations or metastable phases. Ternary alloys were given a standard solutionizing & aging treatment to facilitate γ' precipitation. To prevent oxidation of samples during heat treatment, all alloys were encapsulated in vacuumed ($5x10^{-3}$mbar) quartz tube and heat treated in furnace (Figure 2-16).

Figure 2-16 Heat treatment furnace.

3.4. X-Ray Diffractometry

Phase analysis of as-cast and heat-treated states of all alloys were done by using Bruker D8 Advance XRD diffractometer. Cu Kα radiation was used during the analysis in the diffraction angle (2θ) range of 10-110° with a scanning rate of 0.1°/minutes.

3.5. Differential Scanning Calorimetry

In order to investigate the transformation reaction temperatures of binary and ternary alloy systems, DSC analysis were performed. These thermal analyses were performed by using Setaram Setsys 16/18 DSC. Analyzes were carried out at 10 °C /min heating and cooling rate.

3.6. Scanning Electron Microscopy

Samples from all alloys were prepared in metallography laboratory for microstructural characterization. They were ground up to 2000 grit and polished with alumina. Binary alloys were etched with 50% HCl+ 50% HNO_3 for 10 seconds. Ternary alloys were etched with Marble's reagent for 5 seconds. SEM observations were made using Fei Nova Nano 430 Field Emission Gun device.

3.7. Microhardness Measurement

As-cast and heat-treated states of all alloys were taken by using Shimadzu Micro Hardness Tester with the load of 0.5 kgf. 15 points were taken from each sample to ensure enough sample size.

CHAPTER 4

RESULTS AND DISCUSSION

4.1. Production and Characterization of As-Cast Binary Alloys

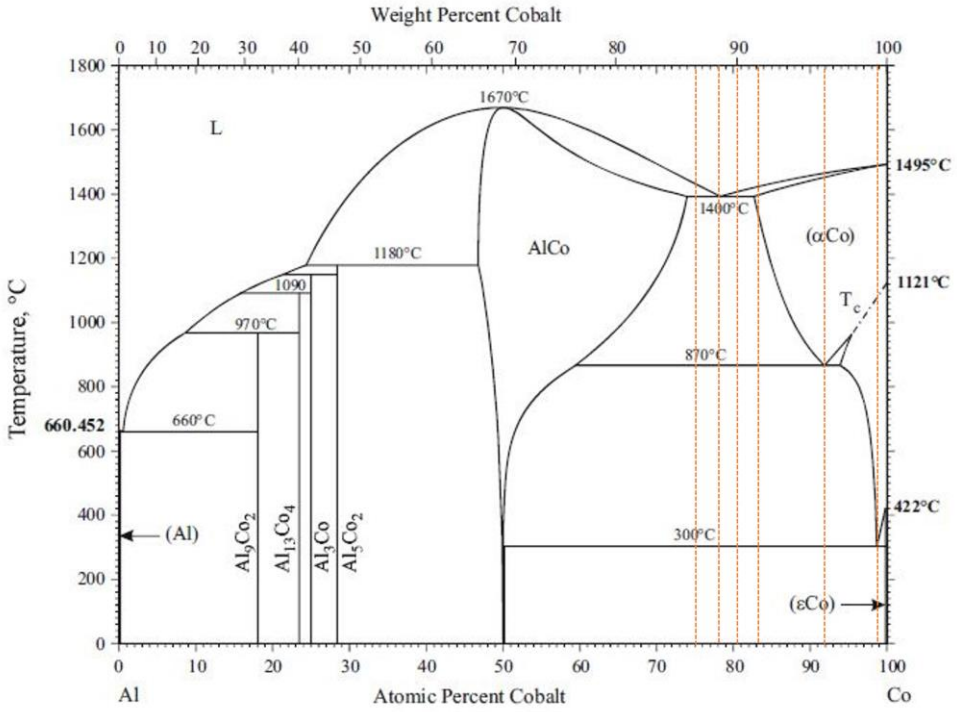

Figure 4-1 Co-Al phase diagram [13].

Six different binary Co-Al alloys were prepared to investigate microstructural properties in as-cast state. Dashed lines on Figure 4-1 denote alloys selected in this work. Since the melting point of Al (660 °C) is much lower than that of Co (1495 °C), some Al loss may occur during melting process. However, weighing results before and after casting given in Table 4-1 show that the Al evaporation during melting is not in significant amounts. It should also be noted that the alloys were not in equilibrium due to relatively fast cooling obtained in arc-melting method. Invariant points were first selected according to the phase diagram. Analyses of those invariant points led to further selection of three other compositions to better understand the Co rich side of Co-Al binary system.

Table 4-1 Weight measurements before & after binary castings.

Alloy	**Weight Before Casting (gram)**	**Weight After Casting (gram)**	**% Loss in Weight**
1.23 at. % Al	8.82517	8.82225	0.03
8.40 at. % Al	8.76684	8.76542	0.02
16.72 at. % Al	9.19383	9.18713	0.07
19.50at. % Al	10.26515	10.26020	0.05
21.50 at. % Al	9.06813	9.06716	0.01
25.00 at. % Al	9.72725	9.71985	0.08

Semispherical geometries (also called buttons) were obtained after solidification. The reasoning behind is that they tend to minimize their surface area to volume ratio. Slices were used to get optical and SEM micrographs, perform XRD analysis and microhardness measurements.

4.1.1. Phase Analysis

Phase analyses of binary as cast Co_xAl_{1-x} alloys have been carried out by XRD technique. XRD results of as cast state of the alloys are given in Figure 4-2 for pure Co and low Al containing alloys together and in Figure 4-3 for high Al containing alloys.

As-cast XRD results indicate that low Al containing alloys (1.23 and 8.40 at. % Al) consist of single phase ϵ-Co as opposed to what binary Co-Al phase diagram shows where ϵ-Co is supposed to coexist with B2-CoAl. However, it is known that Al is not soluble in the stable hcp-Co. This case can be explained by the fact that due to the very limited solid-state diffusion during arc melting procedure, the metastable form of ϵ-Co that has Al solubility at least up 8.40 % at. Al was probably formed in low Al containing alloys as it is explained in Table 2-1. There is also a noticeable shift on peaks of low Al containing alloys especially for 8.40 at. % Al alloy. It indicates that lattice parameter of ϵ-Co is altered due to Al being trapped in its lattice and as more Al is trapped in ϵ-Co peaks shift more.

According to the XRD results of high Al containing alloys (at. % Al ≥ 16.72) given in Figure 4-3, they consist of three phases as α-Co, ϵ-Co, and B2-CoAl. However, these results are not consistent with the Co-Al binary phase diagram (Figure 4-1) where ϵ-Co and B2-CoAl are supposed to coexist up to ~50 at. % Al. It is also apparent that Gibbs' Phase Rule does not agree with the XRD results of high Al containing alloys as well. Gibbs' Phase Rule states that three phases cannot coexist for any binary alloy except for an invariant or transformation point. Therefore, α-Co can be described as untransformed structure in as-cast state which is expected to decompose into ϵ-Co and B2-CoAl phases by eutectoid reaction at around 300 °C.

To sum up the phase analysis for all binary systems, it seems Co-Al binary system does not agree, as expected, with as-cast state where non-equilibrium solidification took place. For this reason, to ensure homogenization and obtain equilibrium structure annealing heat

treatment was carried out for 24 hours at 1300 °C. Their results will be given in following chapters.

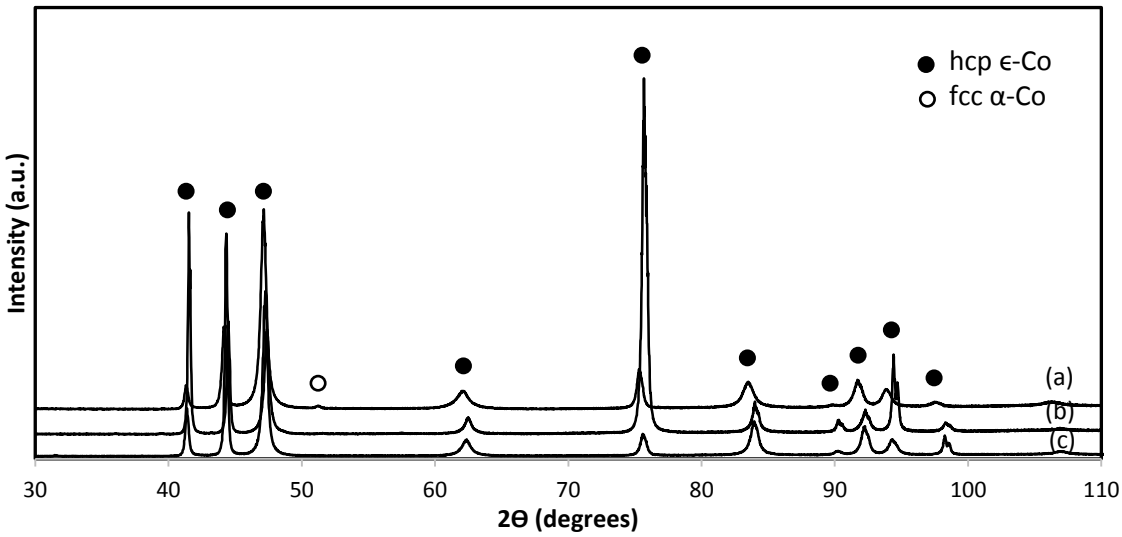

Figure 4-2 XRD patterns of pure Co and low Al containing alloys in as cast state (a) 8.20 at.% Al, (b) 1.23 at. Al, (c) Pure Co.

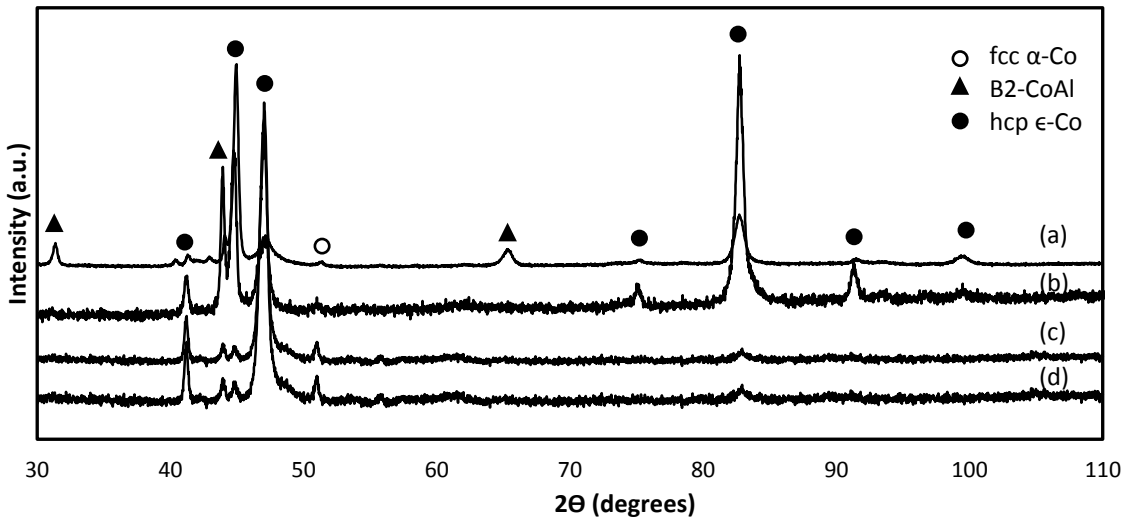

Figure 4-3 XRD patterns of high Al containing alloys in as cast state a) 25 at. % Al, b) 21.50 at. % Al, c) 19.50 at. % Al, d) 16.72 at. % Al.

4.1.2. Thermal Analysis

Figure 4-4 shows DSC curves for low Al containing alloys on heating. These curves do not show any peak. Figure 4-5 shows small endothermic peak occurs at 1368 °C on heating for 19.5 and 21.5 at. % Al alloys. This peak possibly indicates an order-disorder transformation from B2-CoAl to A2-CoAl. Although there is no data given in the literature for order-disorder transformation of CoAl, aluminides such as FeAl shows very high order-disorder transformation temperature very close to its melting point [104]. However, this transformation could not be observed in 16 and 25 at. % Al binary alloys.

DSC cooling curves of high Al containing alloys do not indicate any fcc-Co to hcp-Co+B2-CoAl eutectoid transformation at around 300 °C as shown in Figure 4-6. On the other hand, DSC curves of 1.23 at. % Al and 8.40 at. % Al given in Figure 4-7, indicate that 1.23 at. % Al undergoes a transformation from fcc-Co to hcp-Co via martensitic

manner while there was no such visible transformation for 8.40 at. % Al. This transformation is unique in a way that Co transformation from fcc to hcp can occur via martensitic way not requiring very high cooling rates. It may even occur in furnace cooling [23].

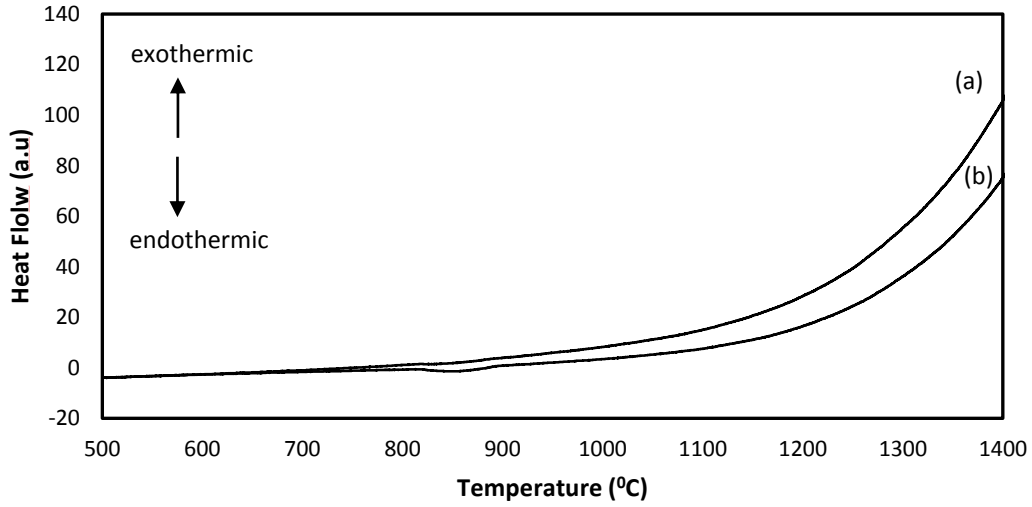

Figure 4-4 DSC curves of (a) 1.23 at % Al, (b) 8.20 at % Al on heating.

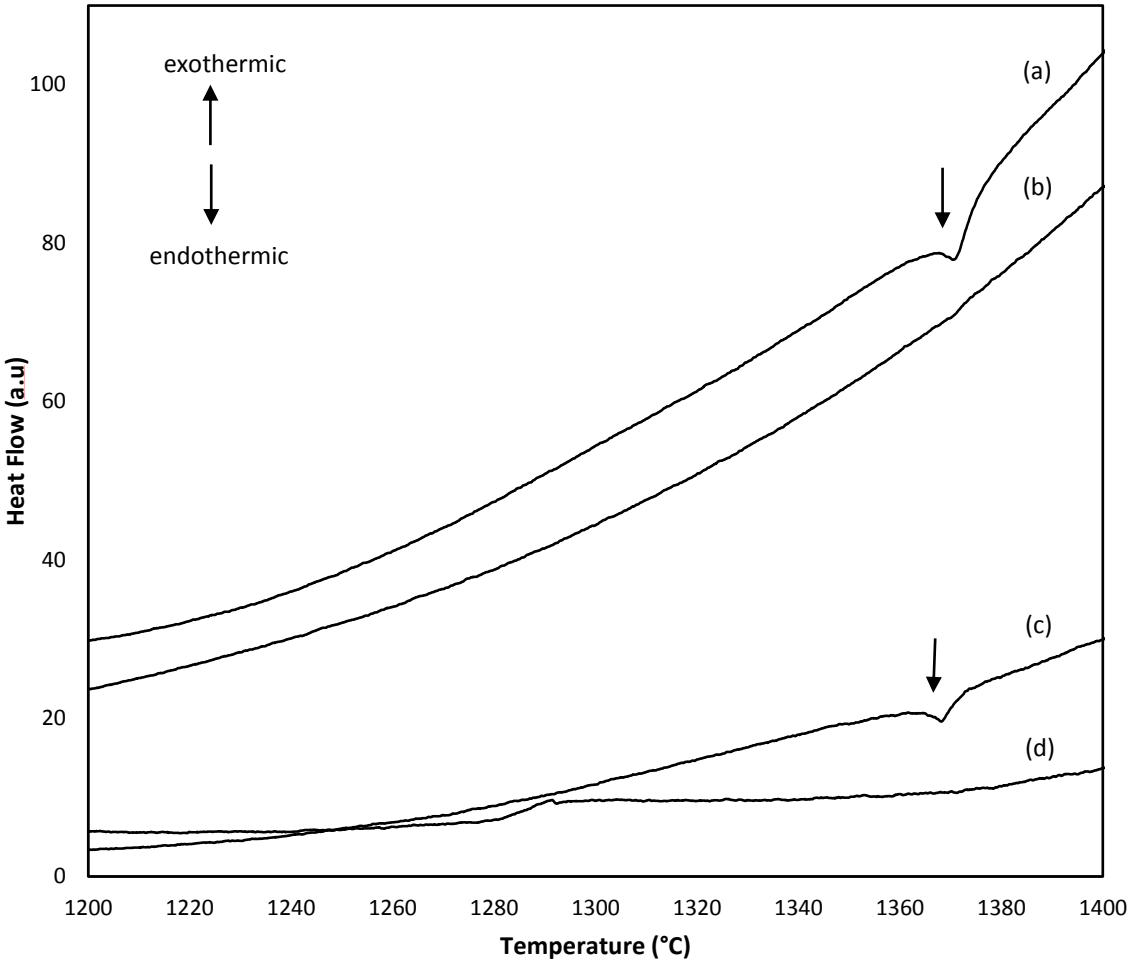

Figure 4-5 B2 to A2 order-disorder transformation for CoAl (a) 21.50 at % Al, (b) 16.72 at % Al, (c) 19.50 at % Al, (d) 25 at % Al on heating.

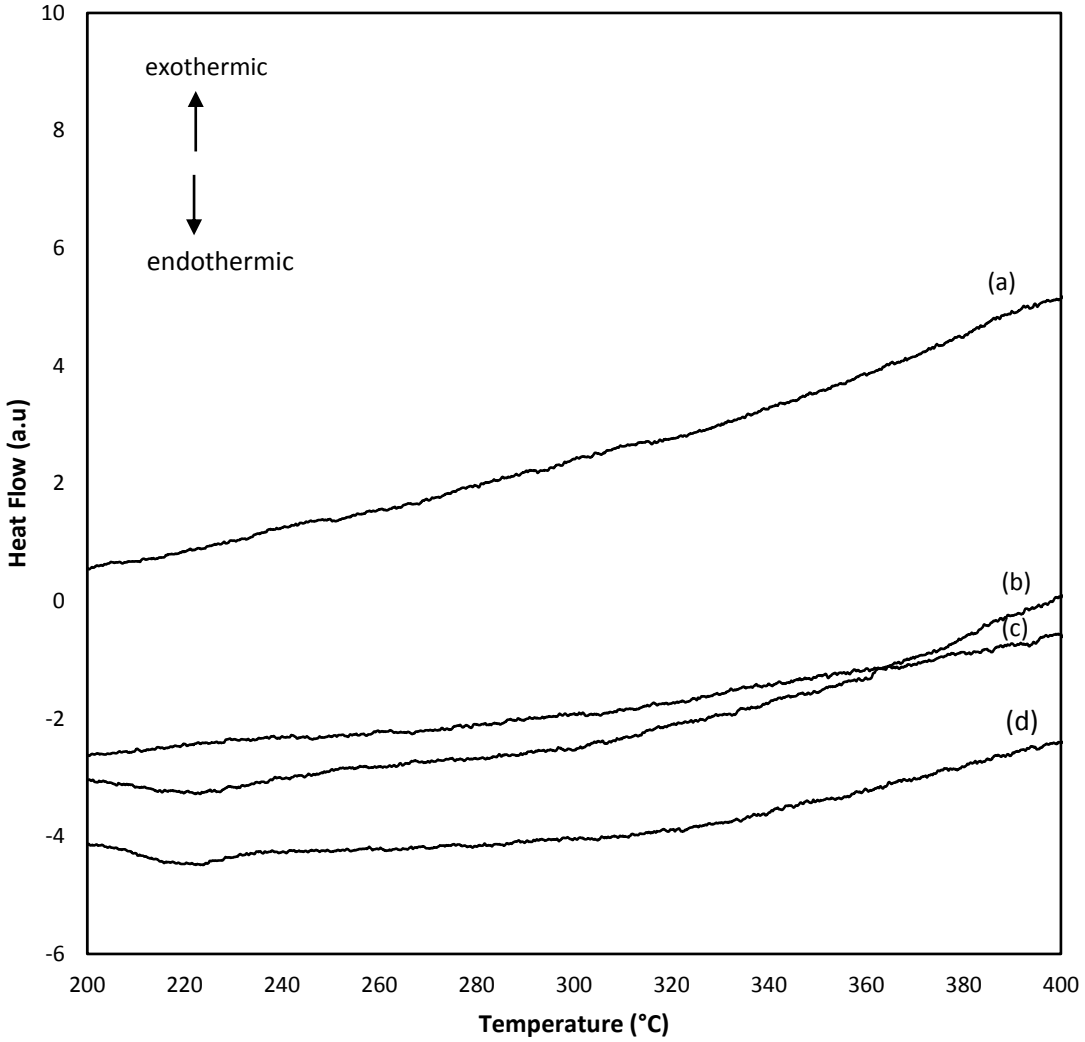

Figure 4-6 No Eutectoid or martensitic transformation from fcc Co to hcp Co (a) 25 at % Al, (b) 19.50 at % Al, (c) 21.50 at % Al, (d) 16.72 at % Al on cooling.

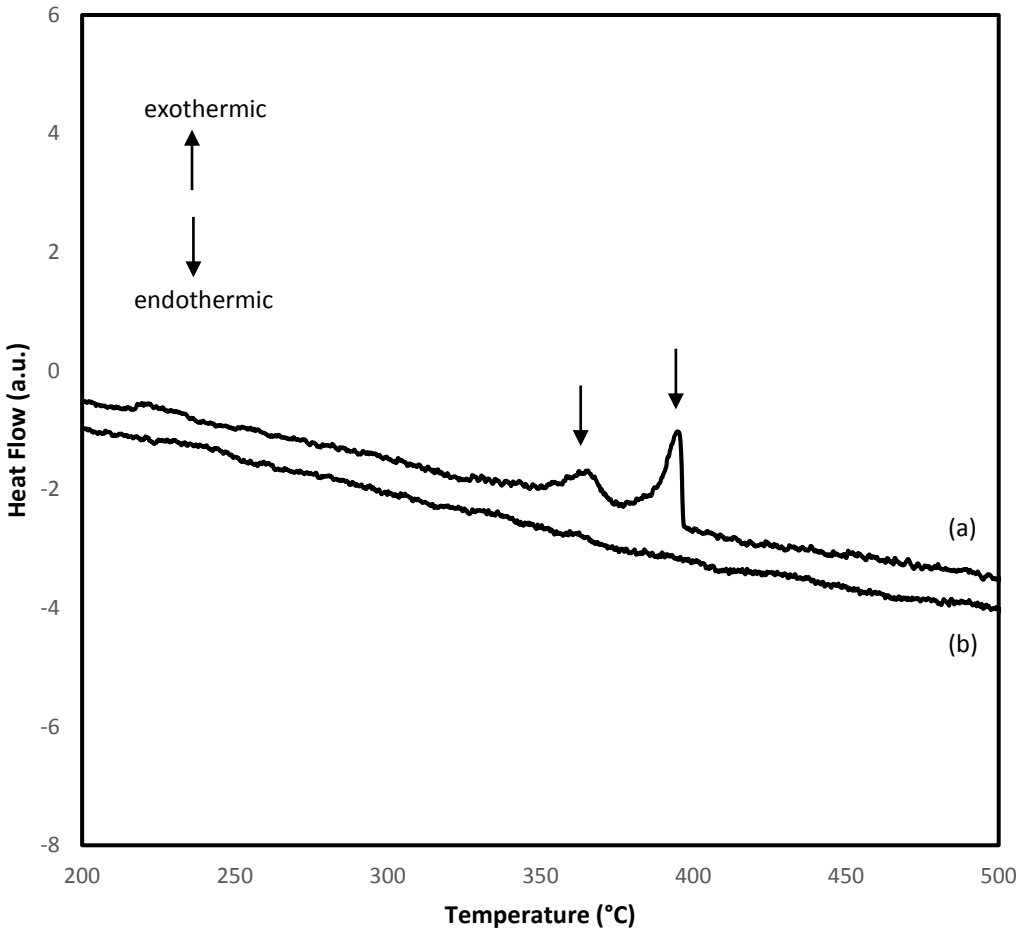

Figure 4-7 Martensitic transformation from fcc-Co to hcp-Co seen in (a) 1.23 at. % Al, not seen in (b) 8.20 at % Al on cooling.

4.1.3. Microstructural Investigation

In order to investigate microstructural characteristics of Co_xAl_{1-x} binary alloys, FESEM analyses have been carried out (Figure 4-8). Results show that there is no noticeable effect of the solidification cooling rate on the phases present across the sample solidification direction. While the low Al alloys showed dendritic solidification (cellular dendritic for 1.23 at. % Al alloy & columnar dendritic for 8.40 at. % Al alloy), high Al alloys crystallized into the transformed eutectic structure with faceted primary phase.

XRD results agree well with the FESEM results to begin with. Low Al containing alloys have single phase hcp-Co in their microstructure. Any observable peak indicating CoAl phase was not detected. In this case, it can be said that all the Al is in solid solution within hcp-Co lattice. Conversely, high Al binary alloys show distinct eutectic morphology with hcp-Co+B2-CoAl transformed eutectic mixture between faceted primary fcc-Co solid solution dendrites. As the eutectic point is approached by increasing the Al content in the binary alloys, the volume fraction of the eutectic mixture increases accordingly. For all the high Al containing alloys EDS results show that primary fcc-Co phase has ~17 at. % Al which equals to maximum amount of Al that can be in solid solution within fcc-Co lattice. Eutectic mixture has average Al content between 30 and 38 at. % Al depending on Al content of binary alloy.

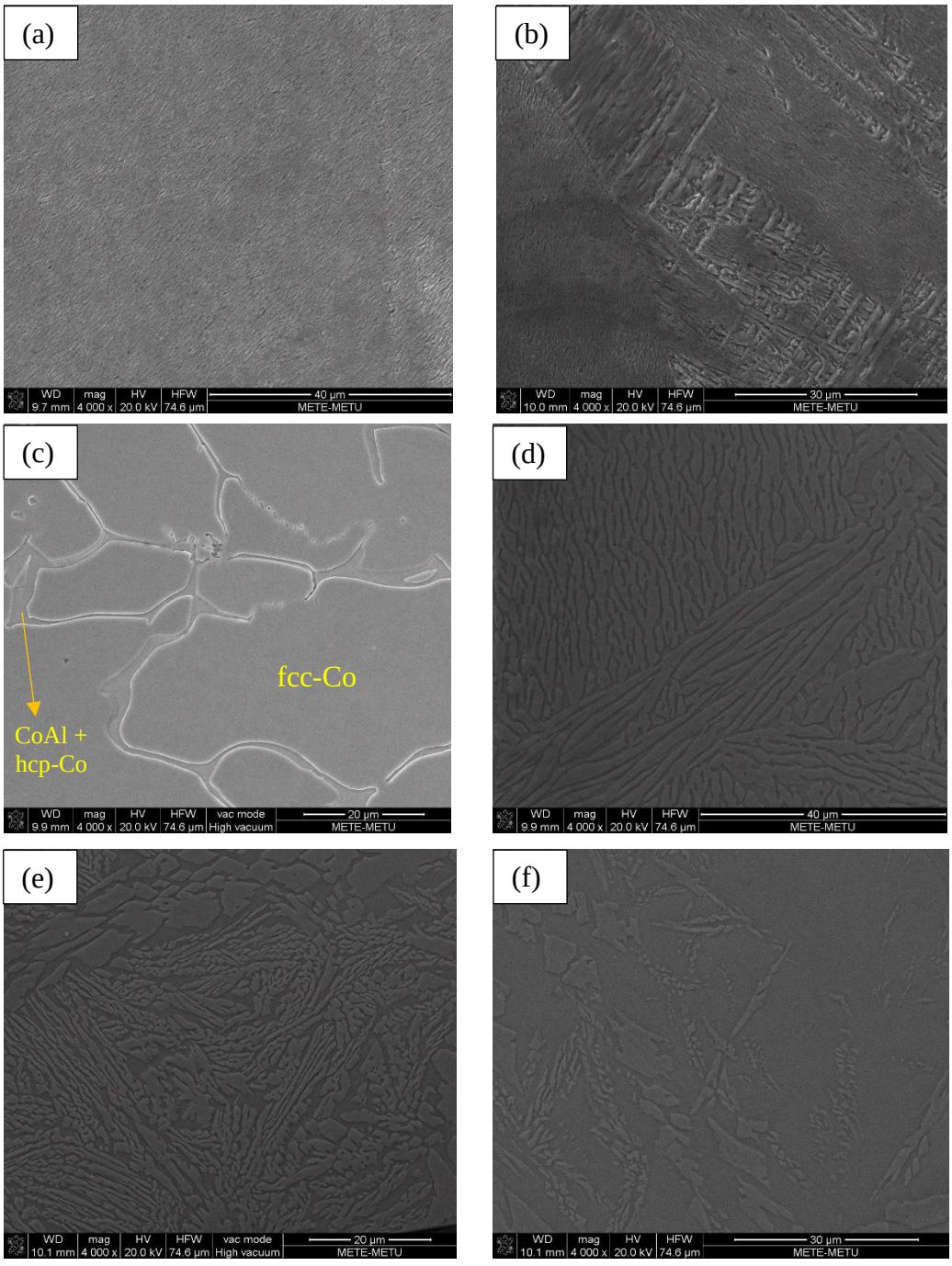

Figure 4-8 FESEM micrographs of as cast (a) 1.23, (b) 8.40, (c) 16.72, (d) 19.50, (e) 21.50 and (f) 25 at. % Al binary alloys.

4.2. Production and Characterization of As-Cast Ternary Alloys

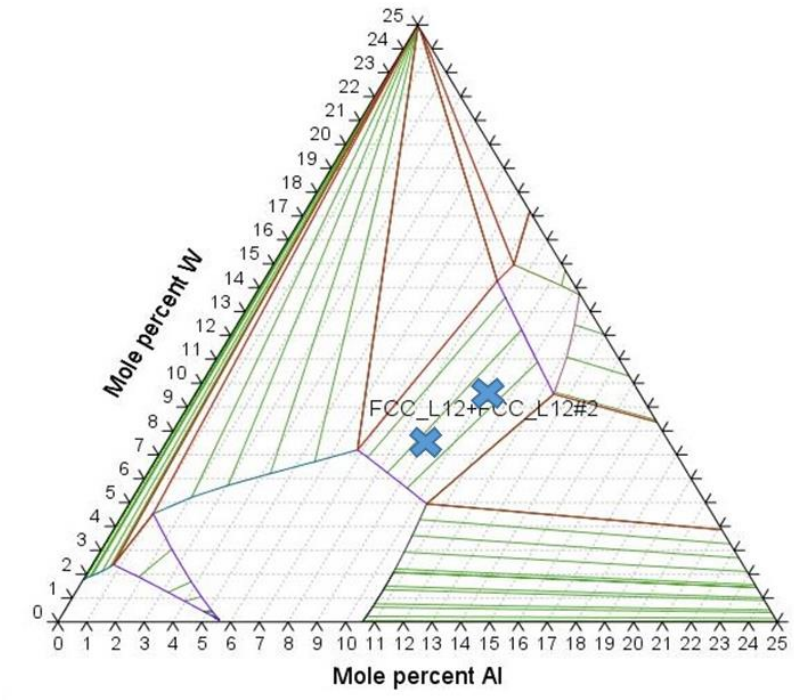

Figure 4-9 Selected ternary compositions in this framework.

Since Co-Al binary system does not yield γ/γ′ phase structure, efforts were devoted to achieve γ/γ′ in Co-Al-W ternary system. For this purpose, Co-19.5Al and Co-16.7Al binary alloys were taken as base system and some of Al was substituted by W. Two ternary alloys having composition of Co-10Al-9.5W and Co-9Al-7.5W alloys were prepared and cast in arc-melting considering the ternary phase diagram of Co-Al-W at 900 °C (Figure 4-9). Points marked by crosses on the diagram show that the two chosen ternary alloy compositions that may form γ/γ′ phase structure at 900 °C. By drawing tie lines, it was calculated that Co-10Al-9.5W alloy to contain 70 % γ′ whereas Co-9Al-7.5W alloy to contain 26% γ′. On the other hand, when the ternary phase diagram at 25 °C (Figure 4-10)

is examined, fcc-Co + B2-CoAl and D019-Co_3W are the stable phases at selected points. Therefore, it is possible to say that γ/γ′ structure is metastable and can decompose into stable phases mentioned above.

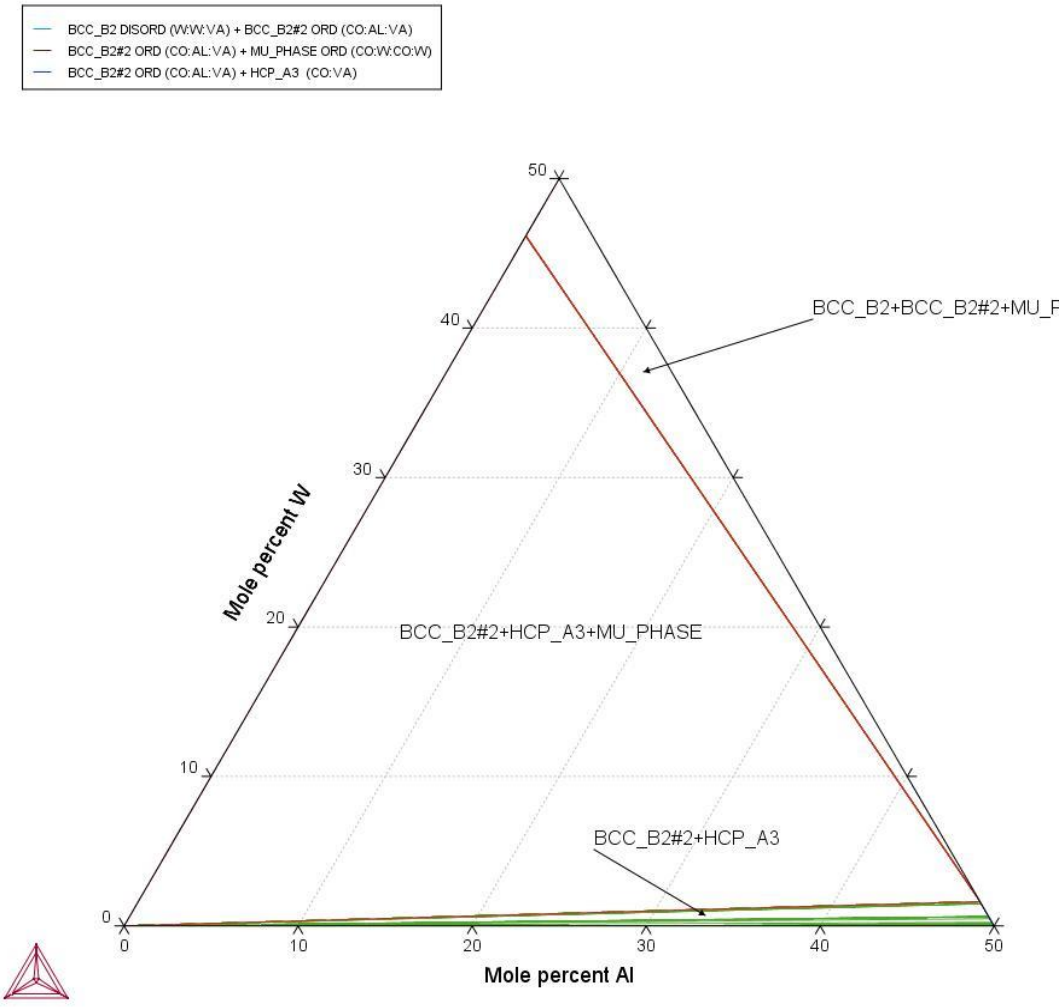

Figure 4-10 Co-Al-W phase diagram at 25 °C.

Table 4-2 shows the weight measurements before and after casting. Due to tungsten having much higher melting point that Al, weight loss is higher than what was obtained in binary castings.

Table 4-2 Weight measurements before & after ternary castings.

Alloy	Weight Before Casting (gram)	Weight After Casting (gram)	% Loss in Weight
Co-10Al-9.5W	11,49609	11,44284	0,46
Co-9Al-7.5W	10,72792	10,67349	0,51

4.2.1. Phase Analysis

Phase analyses of both ternary as cast Co-Al-W alloys have been carried out by XRD technique. Figure 4-12 and Figure 4-13 show diffraction peaks of the constituent phases (α-Co and Co_9W) for both ternary alloys. Results revealed out that phases in as-cast structure do not agree with the current ternary phase diagram of Co-Al-W where B2-CoAl, ϵ-Co, and Co_3W are supposed to coexist. It is observed that fcc-Co and Co_9W present for both ternary alloys. This mismatch with the phase diagram, again, due to non-equilibrium nature of arc melting procedure. In literature, there is no information indicating that Co_9W intermetallic can be found as a stable phase. As also can be seen in Co-W phase diagram (Figure 4-11) [105] given below, fcc-Co and Co_9W phases are not present as equilibrium phases at room temperature.

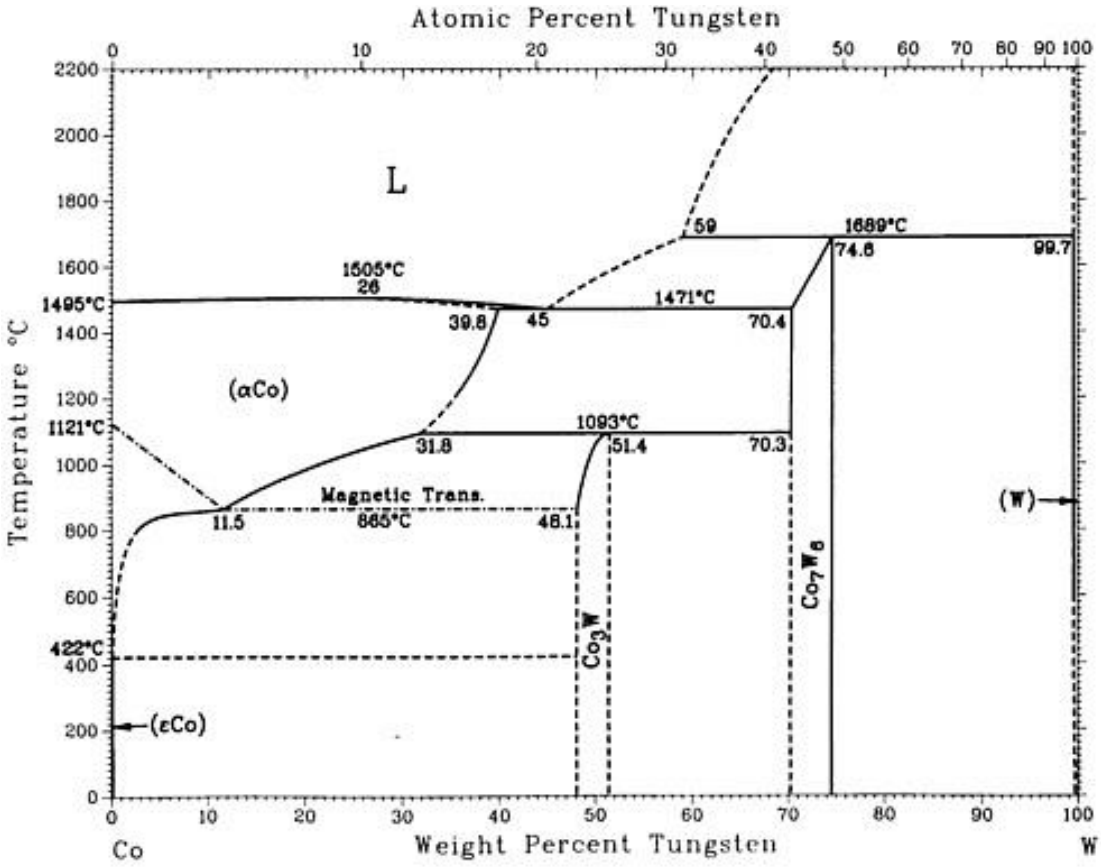

Figure 4-11 Co-W phase diagram [105].

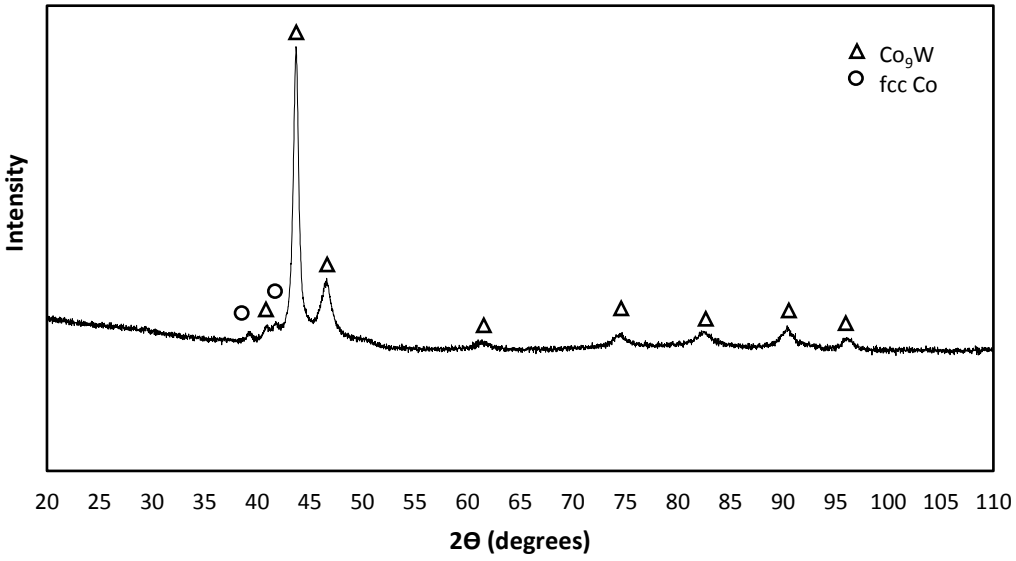

Figure 4-12 XRD pattern of as cast Co-10Al-9.5W ternary alloy.

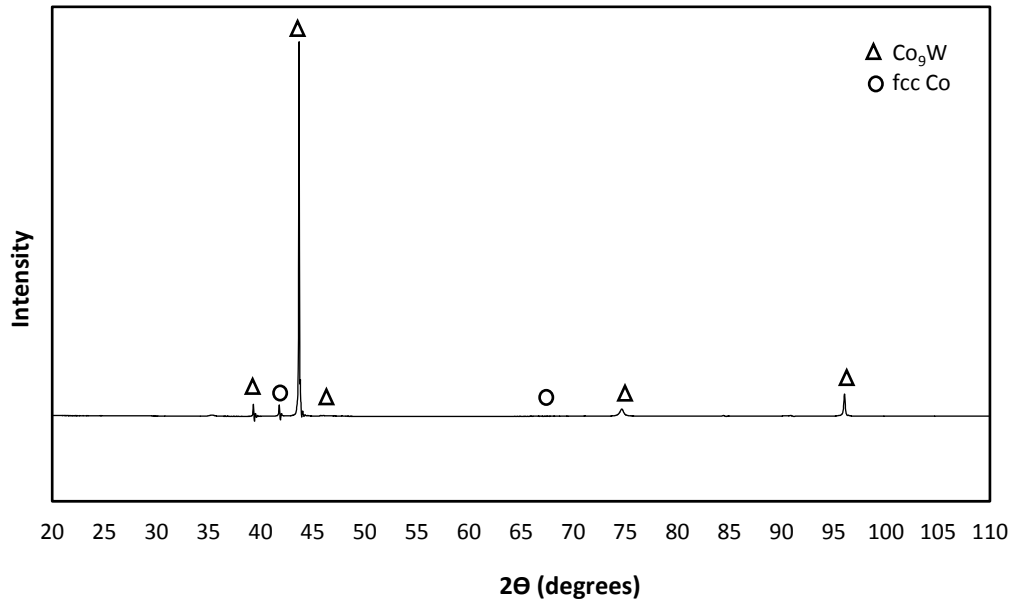

Figure 4-13 XRD pattern of as cast Co-9Al-7.5W ternary alloy.

4.2.2. Thermal Analysis

DSC heating and cooling curves of both ternary alloys show very similar peaks (Figure 4-14 & Figure 4-15). On cooling, an exothermic peak at around 1000 °C was observed (Figure 4-14) that is supposed to coincide with γ' solvus temperature. Figure 4-15 shows similar peak however at lower temperatures (~920 °C). It is important to note that γ' solution temperature increases with the both Al and W content.

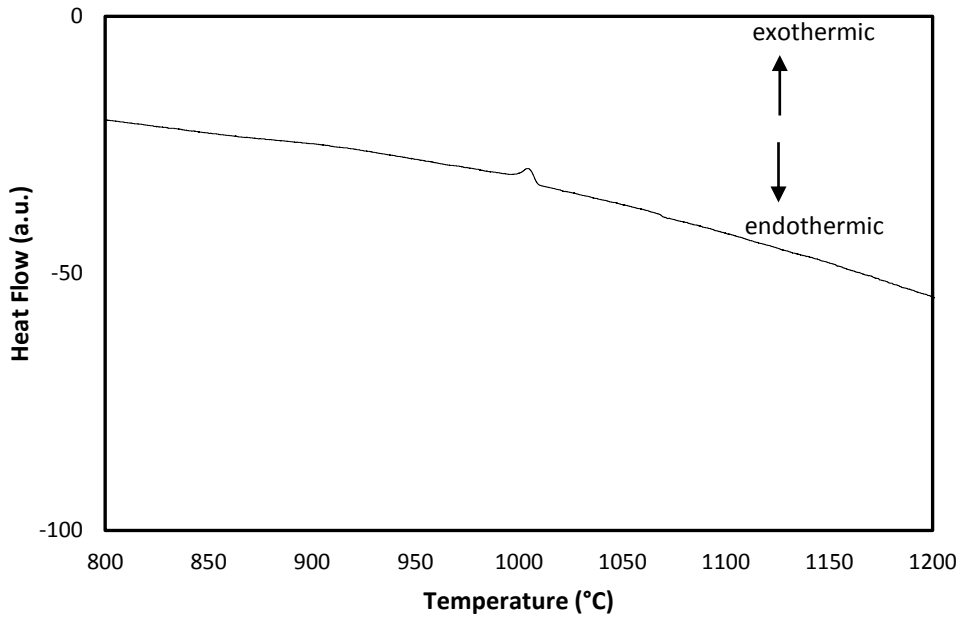

Figure 4-14 DSC cooling curve of Co-10Al-9.5W alloy.

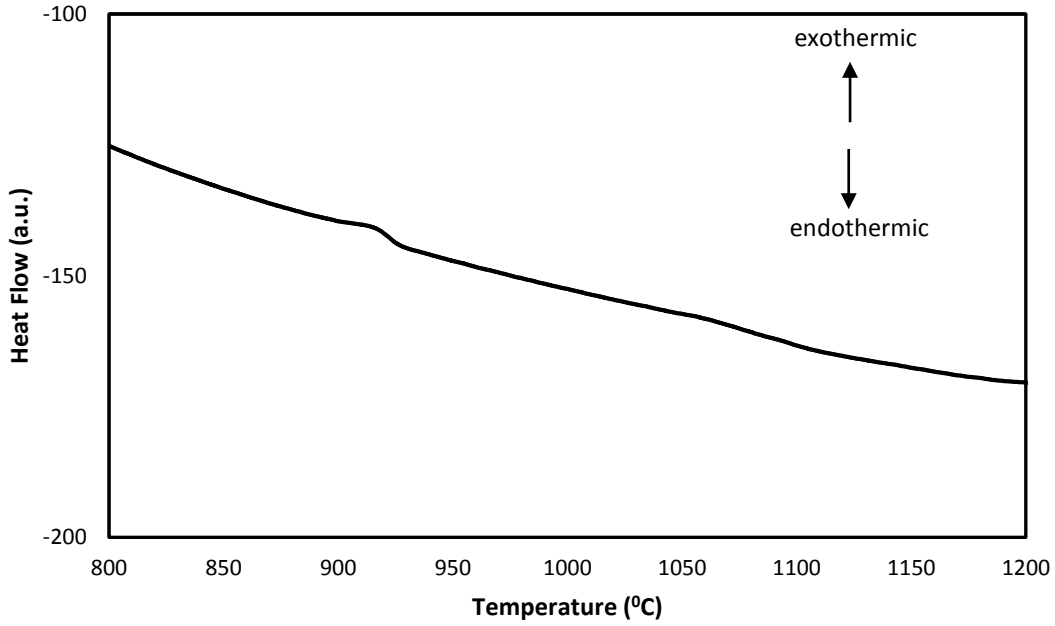

Figure 4-15 DSC cooling curve of Co-9Al-7.5W alloy.

4.2.3. Microstructural Investigation

FESEM observations of both ternary alloys show two-phase microstructure (Figure 4-16). Phases present are fcc stabilized Co matrix and Co_9W intermetallic precipitate at dendritic cores. The reason behind this can be explained by the fact that, during solidification of Ni or Co-based superalloys containing different melting point alloying elements, low melting point elements such as Ti, Al or Ta tend to diffuse interdendritic regions whereas high melting point refractory elements such as Mo, W or Re tend to diffuse towards dendritic arms. This leads to enrichment of high melting point elements at dendritic regions and enrichment of low melting point elements at interdendritic regions. Depending on this, Co_9W intermetallics precipitate at dendrite arms enriched by high melting point elements.

Additionally, this is the main reason for the presence of the γ' precipitation at the interdendritic region in Ni-based superalloys [106] . EDS results are given in Table 4-3.

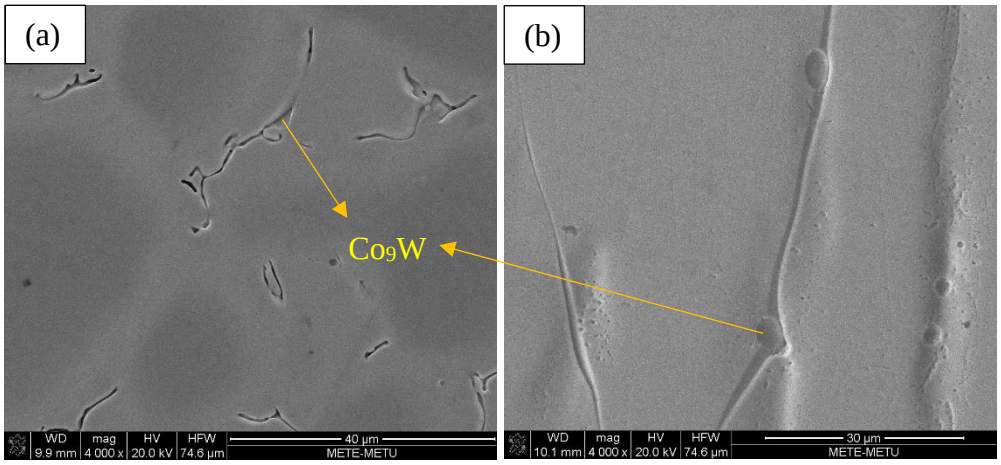

Figure 4-16 FESEM micrographs of as cast (a) Co-10Al-9.5W and (b) Co-9Al-7.5W ternary alloys.

Table 4-3 EDS analyses of phases in as-cast state for ternary alloys

Alloy	Phase	Al at. %	W at. %
Co-10Al-9.5W	γ	14.2	10.1
	Co_9W	-	8.6
Co-9Al-7.5W	γ	11.2	7.1
	Co_9W	-	8.4

4.3. Heat Treatment of Arc-Melted Alloys

The arc-melted samples were subjected to homogenization/solutionizing heat treatment. For binary alloys, this is done to alleviate the non-homogenous nature of arc-melted alloys due to relatively fast crystallization. For ternary alloys, solutionizing and subsequent aging treatments were performed to facilitate γ' precipitation.

4.3.1. Binary alloys

After investigation of binary as-cast samples it seemed necessary to heat treat binary Co-Al alloys because results did not agree with the current phase diagram of Co-Al. A piece of specimen is taken from each of binary alloys and they were separately encapsulated in evacuated quartz tube. Heat treatment was done at 1300 °C as it is shown on phase diagram (Figure 4-17) given below. The choice of temperature was done according to phase diagram and DSC results in which selected temperature should be high enough to ensure faster kinetics whereas should be low enough to avoid any melting. Heat treatment soaking time was 24 hours followed by furnace cooling.

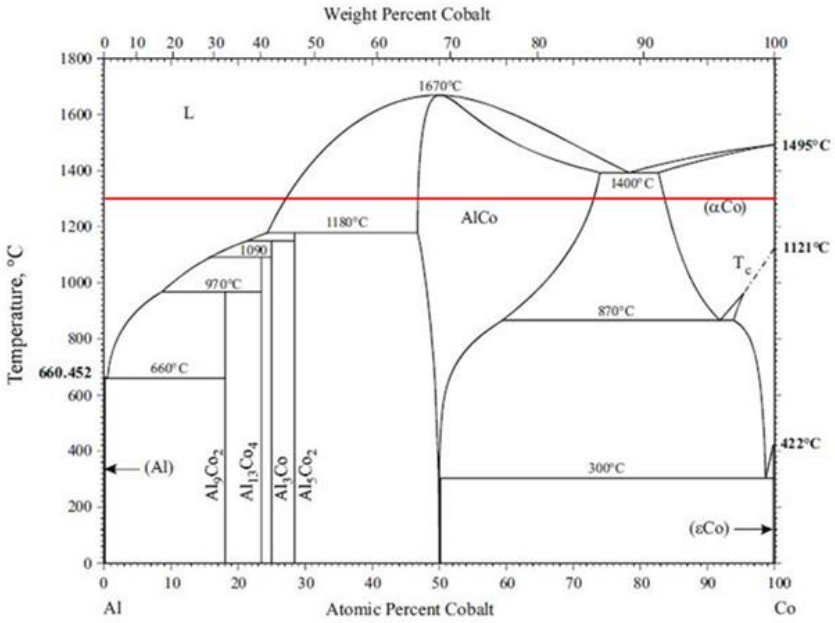

Figure 4-17 Co-Al phase diagram showing the annealing temperature.

4.3.1.1. Phase Analysis

Phase analyses of binary heat-treated Co_xAl_{1-x} were performed to investigate the change in phases present in as cast state. Figure 4-18 and Figure 4-19 denotes the XRD patterns of heat-treated low Al containing and high Al containing alloys, respectively.

What is common for both of alloys is that inevitable oxide peaks emerged even though heat treatment were carried out in vacuumed quartz tubes. Heat-treated XRD results show that CoAl precipitation took place for both low Al containing alloys. However, its intensity is small meaning that very low fraction was precipitated. Nevertheless, this shows a progression towards equilibrium state where fcc-Co will eventually be consumed in favor of hcp-Co and B2-CoAl.

As for high Al containing alloys the number of phases did not change since as-cast state includes all three possible phases.

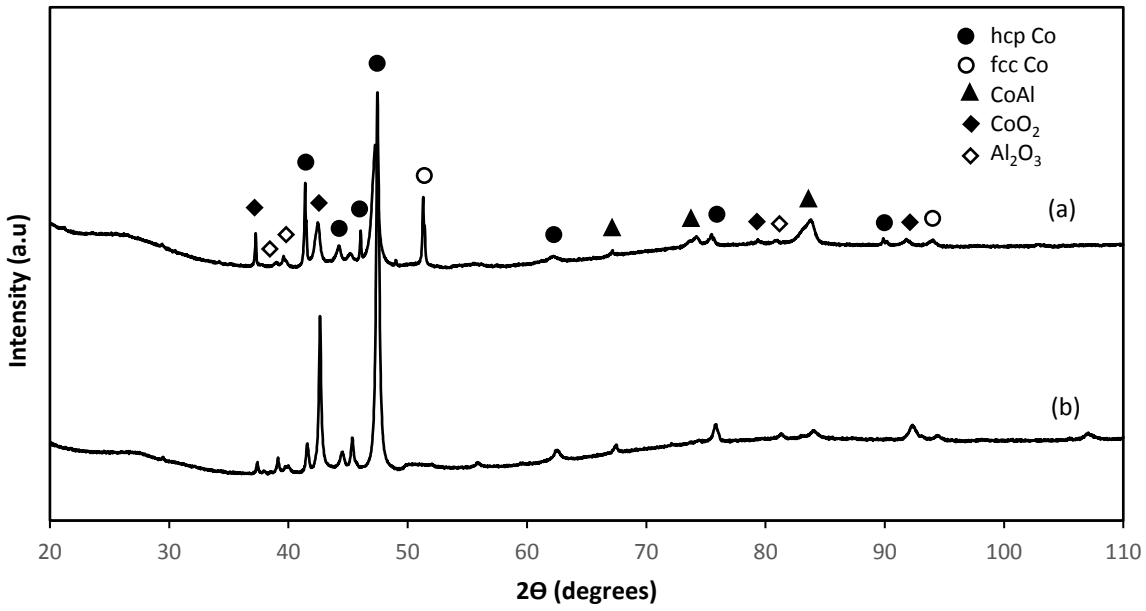

Figure 4-18 XRD patterns of as cast (a) 8.20 at. % Al and (b) 1.23 at. % Al binary alloys.

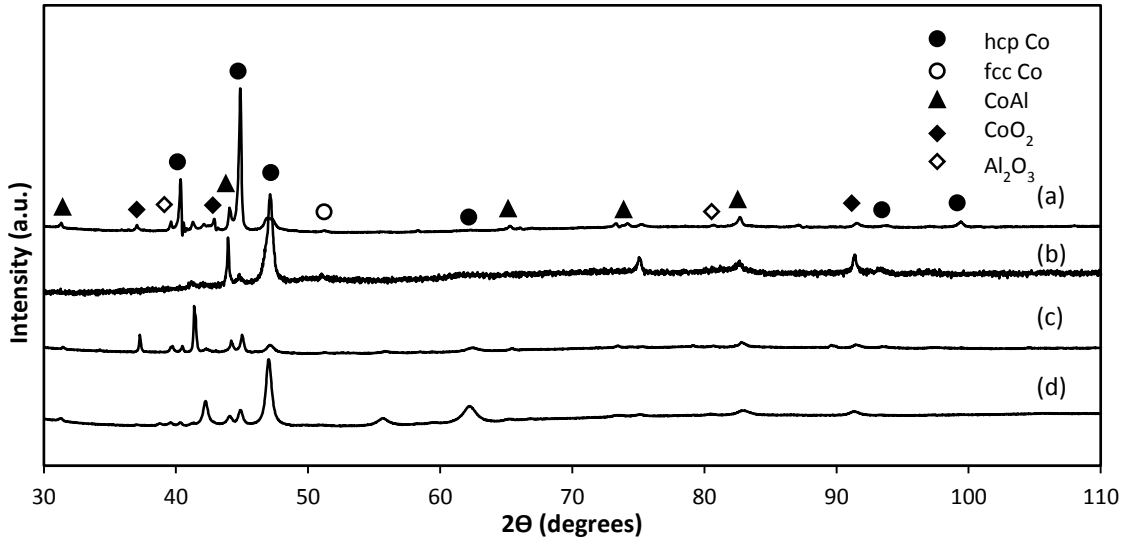

Figure 4-19 XRD patterns of (a) 25 at. % Al, (b) 21.50 at. % Al, (c) 19.50 at. % Al, (d) 1.72 at. % Al binary alloys.

4.3.1.2. Microstructural Investigation

FESEM observations of binary heat-treated alloys show little change compared to as cast state as shown in Figure 4-20. Low Al containing alloys still showed single phase microstructure. Although XRD results showed CoAl peaks, CoAl phase could not be detected through FESEM investigations. This is probably due to CoAl phase having very small precipitate size. High Al containing alloys exhibited 3 phase (fcc-Co, hcp-Co+B2-CoAl mixture) microstructural state. However, volume fraction of fcc-Co phase seemed to diminish by investigation through image analysis in ImageJ program whose results are given in Figure 4-21. As-annealed state still contradicts with Gibb's phase rule as there are 3 phases present in high Al containing alloys. It is postulated that big variation in the solubility of phases that are present in binary state may necessitate even longer annealing times to reach thermodynamic equilibrium.

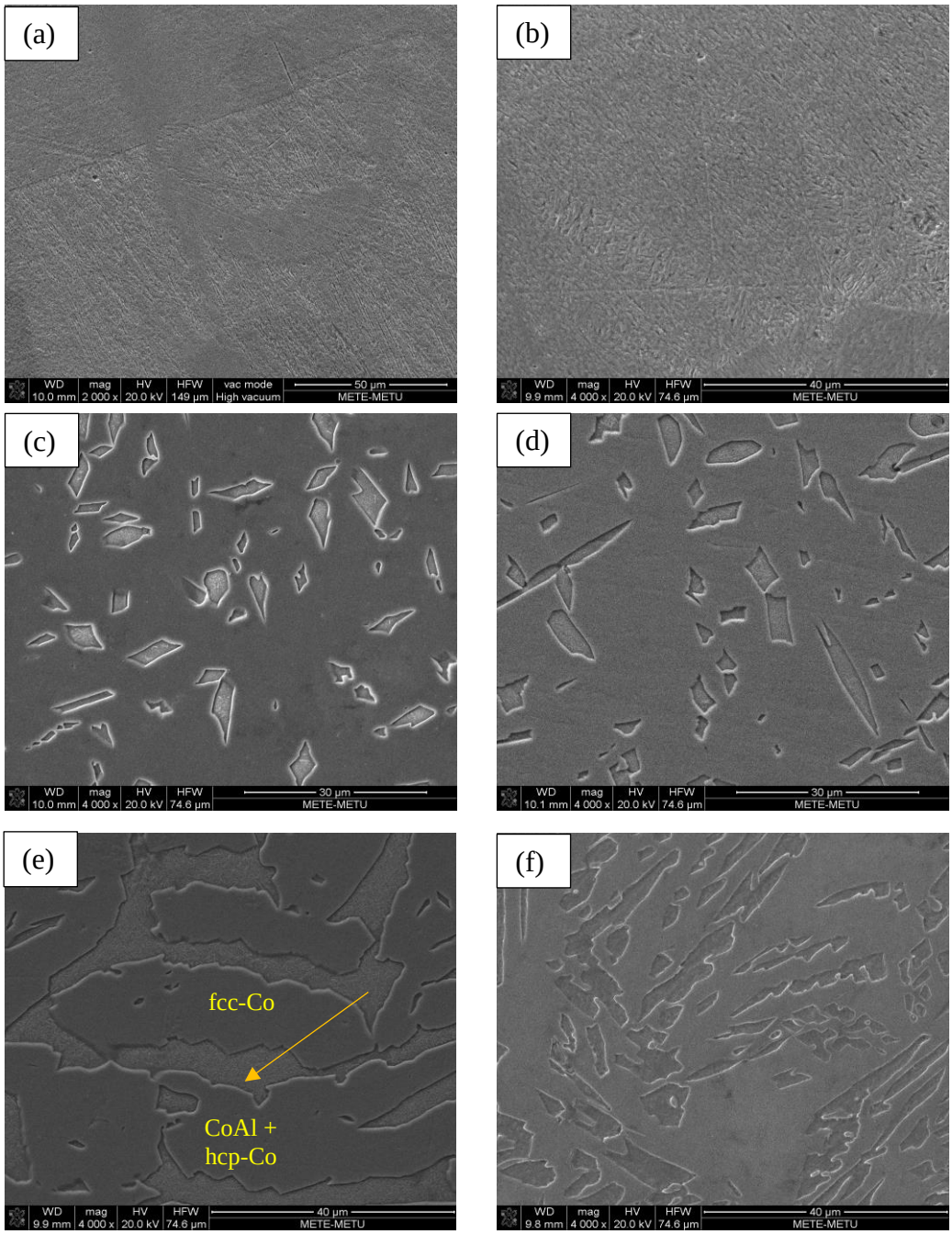

Figure 4-20 FESEM micrographs of heat treated (a) 1.23, (b) 8.40, (c) 16.72, (d) 19.50, (e) 21.50 and (f) 25 at. % Al binary alloys.

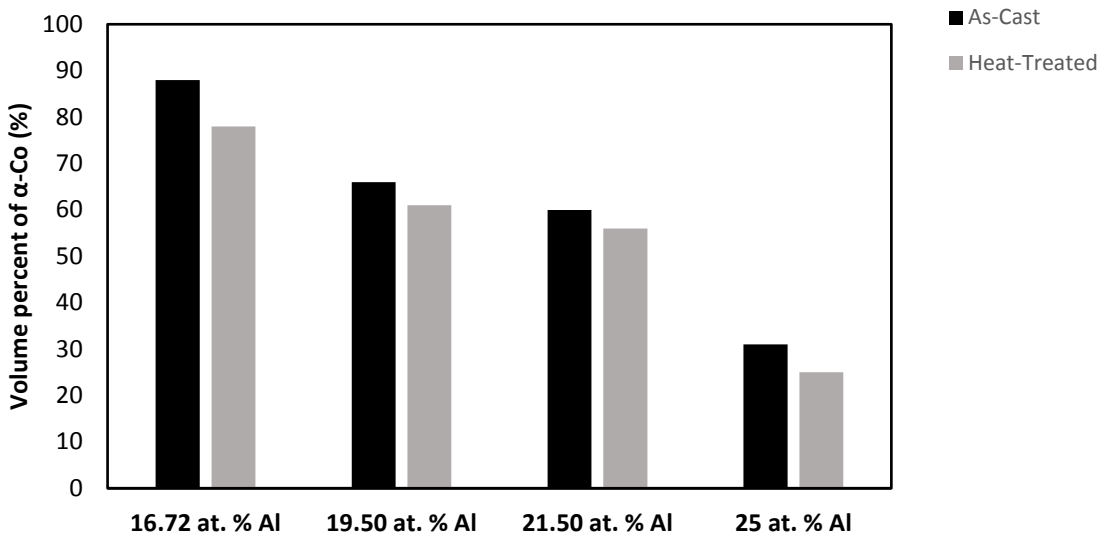

Figure 4-21 Volume fraction change of fcc-Co after heat treatment.

Upon annealing, almost all high Al containing alloys exhibited discontinuous precipitation (Figure 4-22). EDS analyses (Figure 4-23) reveal that their Al composition is lower than fcc-Co phase that surrounds this structure.

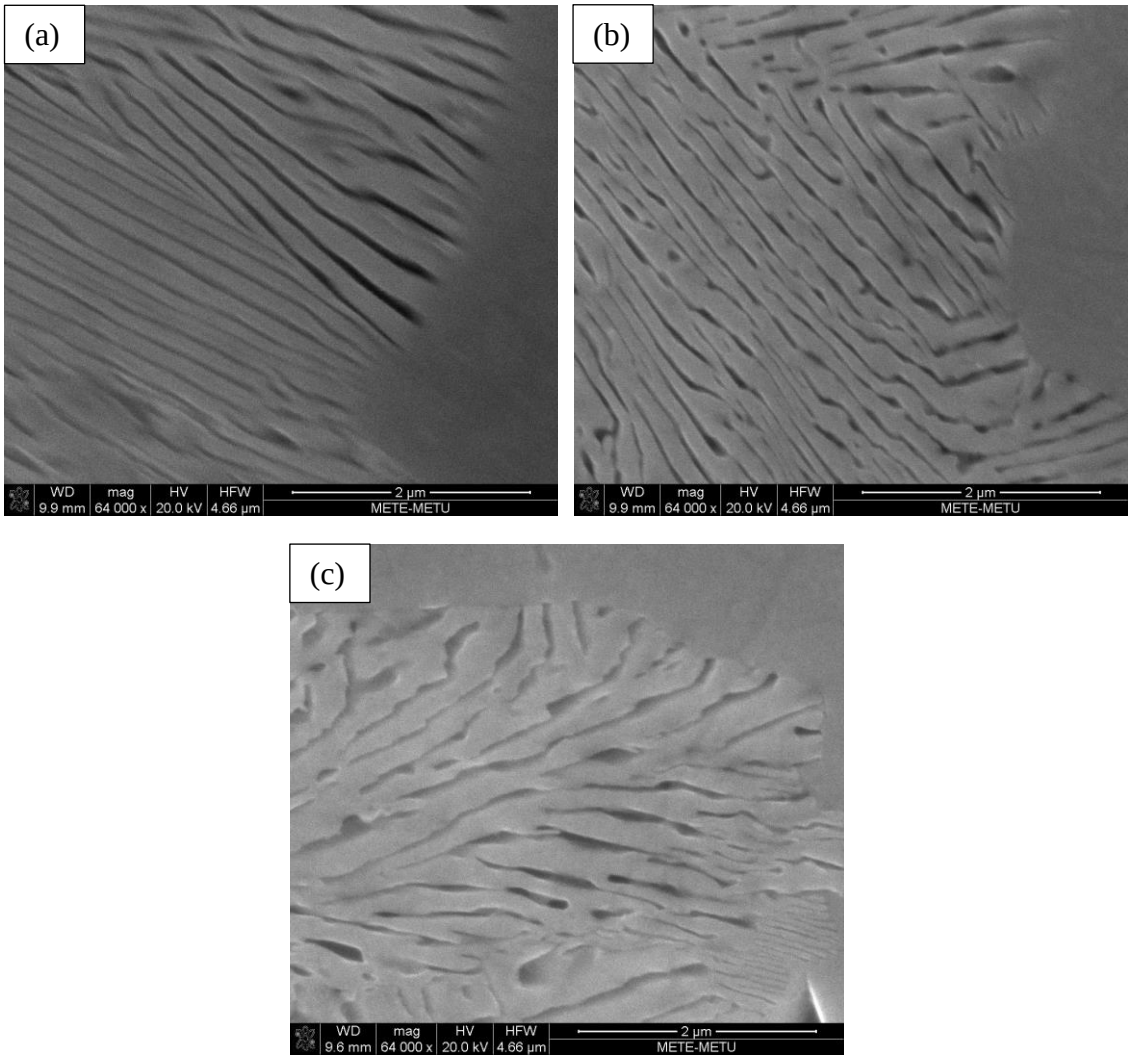

Figure 4-22 Discontinuous precipitation observed upon annealing in (a) 16.7, (b) 19.5 and (c) 21.5 at. % Al alloys.

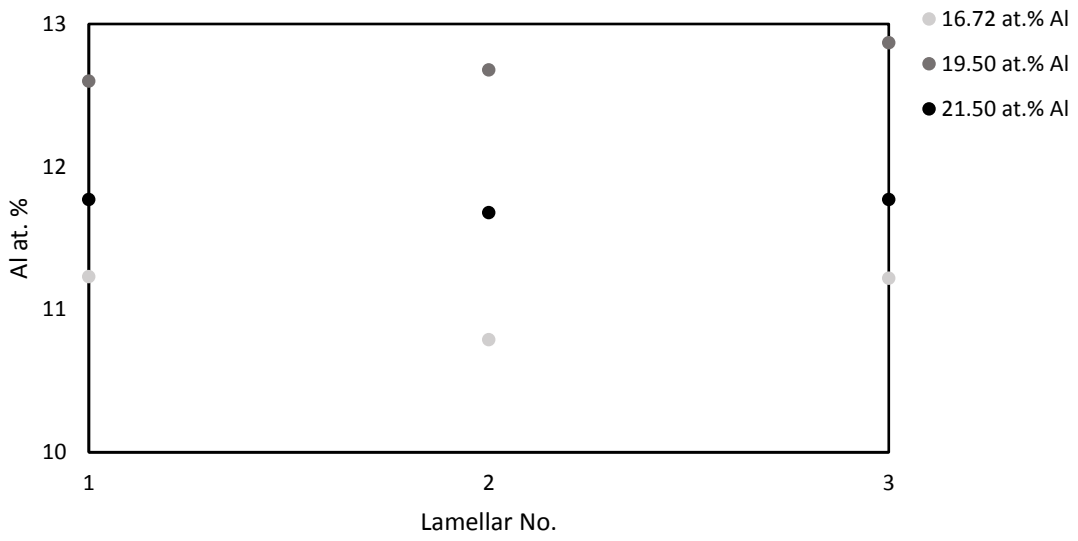

Figure 4-23 at. % Al composition of discontinuously precipitated lamellae at different locations.

4.3.1.3. Microhardness Measurements

Mechanical responses of heat-treated Co_xAl_{1-x} alloy systems have been examined by applying micro-hardness tests. In order to obtain better results, 15 measurements have been applied on each sample and the results have been given in Figure 4-24. Results show that micro-hardness values greatly rely on Al contents especially for high Al containing alloys. This is because as the Al content increase the content of very hard B2-CoAl intermetallic increases in alloys. Increasing CoAl contents directly affect hardness values. As for low Al containing alloys, hardness values become lower than pure Co. This is probably due to Al being softer element compared to Co.

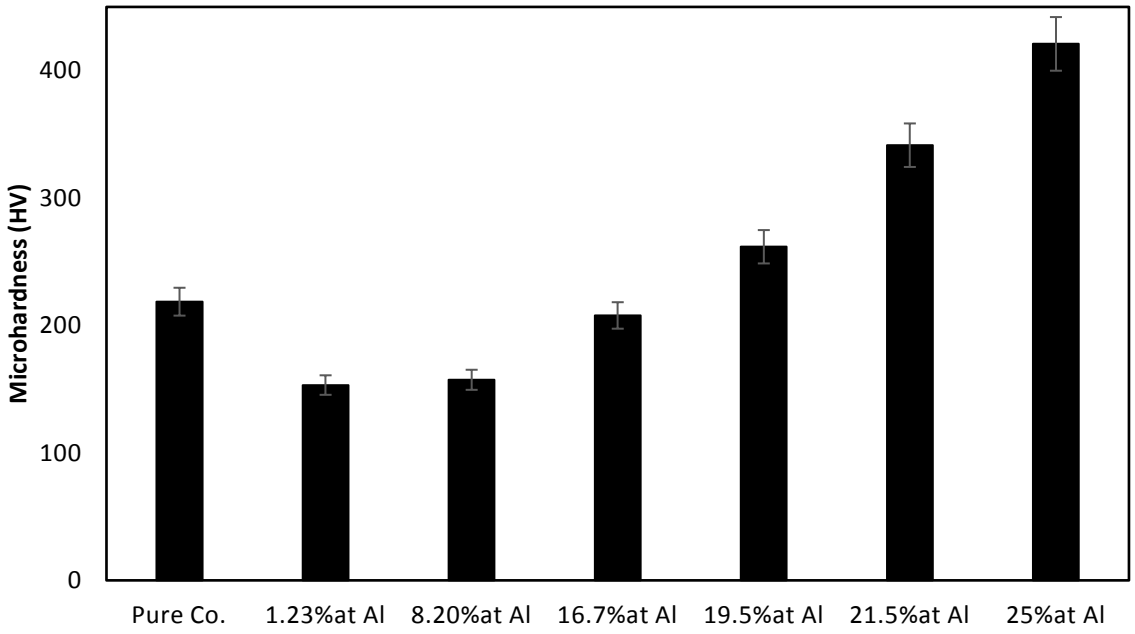

Figure 4-24 Microhardness comparison of pure and alloyed Co.

4.3.2. Ternary alloys

As cast state of ternary alloys do not yield γ' precipitates. Thus, conventional aging procedure was applied. To determine the solutionizing temperature, single phase state (single phase fcc-Co solid solution) must be known. With the help of Thermo-Calc software and using TCNI8 database, ternary phase diagram of Co-Al-W was calculated at 1250 °C (Figure 4-25). Compositions of this work is marked on the phase diagram with the crosses. In order to be on the safe side and obtain faster diffusion kinetics, solutionizing temperature of 1300 °C was applied. The soaking time was 24 hours.

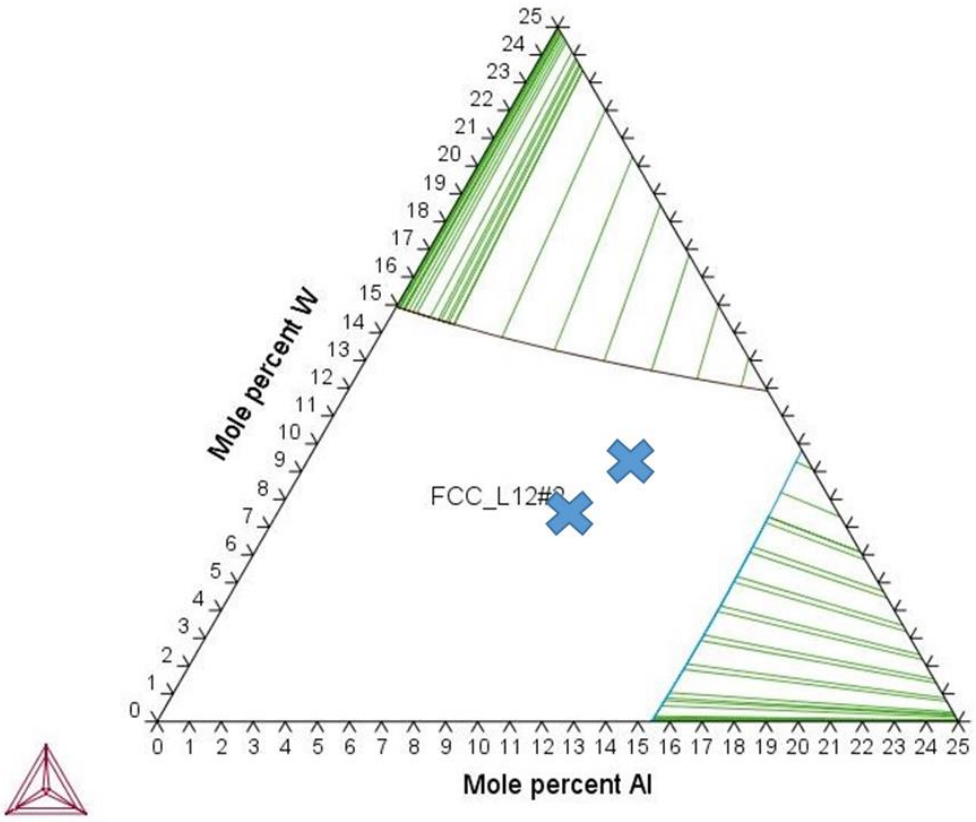

Figure 4-25 Selected compositions crossed on Co-Al-W ternary phase diagram drawn by Thermo-Calc TCNI8 database at 1300 °C.

After soaking was completed, ice-water quenching was applied. Quenched specimens were aged at 900 °C for 16, 64 and 256 hours. Aging temperature was selected by the help of DSC curves and ternary phase diagram drawn by Thermo-Calc for 900 °C. As it can be seen from the figure given above, aging temperature fall on γ/γ' two phase zone.

4.3.2.1. Phase Analysis

Phase analyses of heat-treated ternary Co-Al-W alloys were performed to investigate the phase evolution via aging. Figure 4-26 and Figure 4-27 denote the XRD patterns of aged Co-10Al-9.5W and Co-9Al-7.5W alloys, respectively. Oxide peaks appeared as expected because aging procedure performed under oxidizing atmosphere.

Aged XRD results display existence of γ/γ' dual phase for both ternary alloys. In addition to the classical precipitation hardened superalloy phase structure, additional two intermetallic phases were observed. They are namely Co_3W and Co_7W_6. These phases are unwanted and detrimental to the mechanical properties. The precipitation theory of them is given in microstructural investigation of the aged ternary alloys in the following section.

Since the volume fraction of γ matrix phase within the microstructures is small and lattice constants of fcc-Co(γ) and $L1_2$-Co_3(Al,W)γ' phases are similar to one another, fundamental peaks overlap each other even though XRD scanning rate has been done as slow as 0.1°/minute.

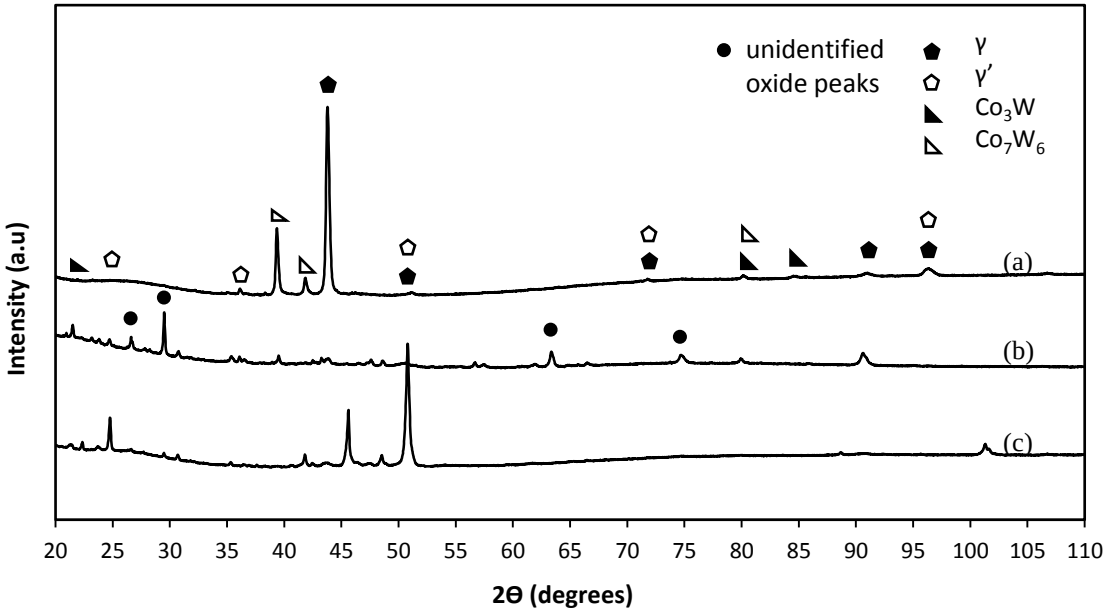

Figure 4-26 XRD patterns of Co-10Al-9.5W aged for (a) 16 h, (b) 64 h, (c) 256 h.

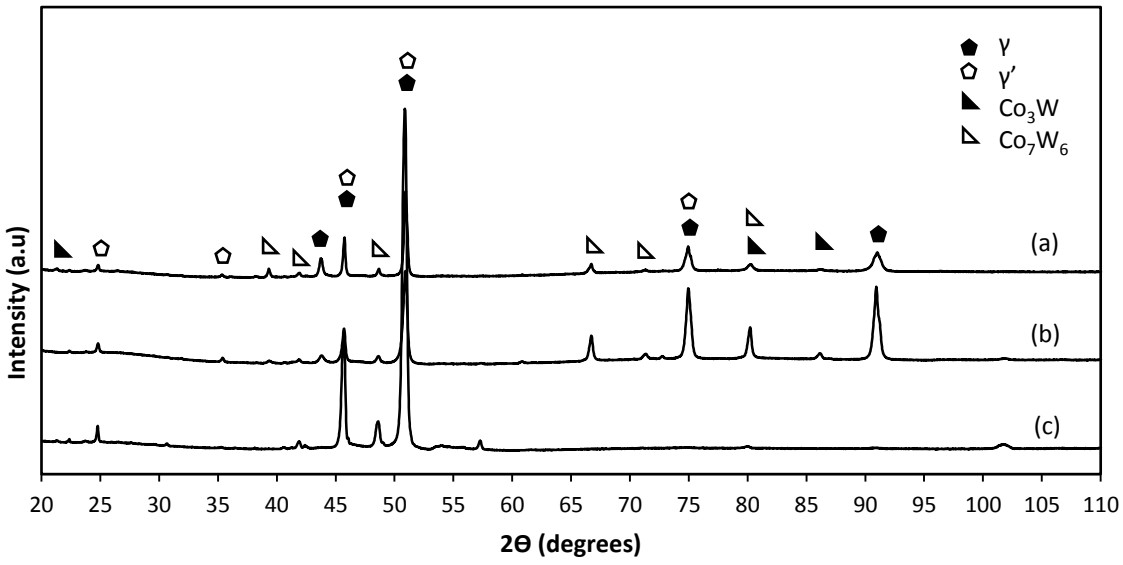

Figure 4-27 XRD patterns of Co-9Al-7.5W aged for (a) 16 h, (b) 64 h, (c) 256 h.

4.3.2.2. Microstructural Investigation

FESEM investigations (Figure 4-28 & Figure 4-29) of aged ternary alloys show distinct γ/γ' two phase microstructures throughout the heat-treated body except for the outermost edges. In 256 hours aged condition, Co-10Al-9.5W alloy has more γ' fraction (~70 %) than Co-9Al-7.5W does contain (~57 %). This is due to the fact that Al & W elements are γ' former elements in Co-based superalloys and the former alloy contains more than the latter. The amount of γ' fraction agrees well with the literature [96, 98, 99, 107] and calculated phase diagram especially for Co-10Al-9.5W alloy. As for Co-9Al-7.5W alloy, since calculated phase fraction ratio does not agree with the phase fraction analysis of aged specimen, Co-Al-W ternary database might need an update. Furthermore, as aging time increases cuboidal γ' fraction increases for both alloys. This can be seen in Figure 4-28(a) and especially in Figure 4-29(a) where γ' start precipitating from supersaturated γ matrix. γ' precipitate size was 200-250 nm for both ternary alloys. This result are also in line with literature [96, 98, 99, 107].

The effect of heat treatment is also seen on grain structure. General microstructure of the both ternary alloys before heat treatment was columnar dendritic type. After heat treatment, they exhibit equiaxed grains containing annealing twins because solution heat treatment was performed at 1300 °C where alloys are in single phase (γ-Co) region for 24 hr.

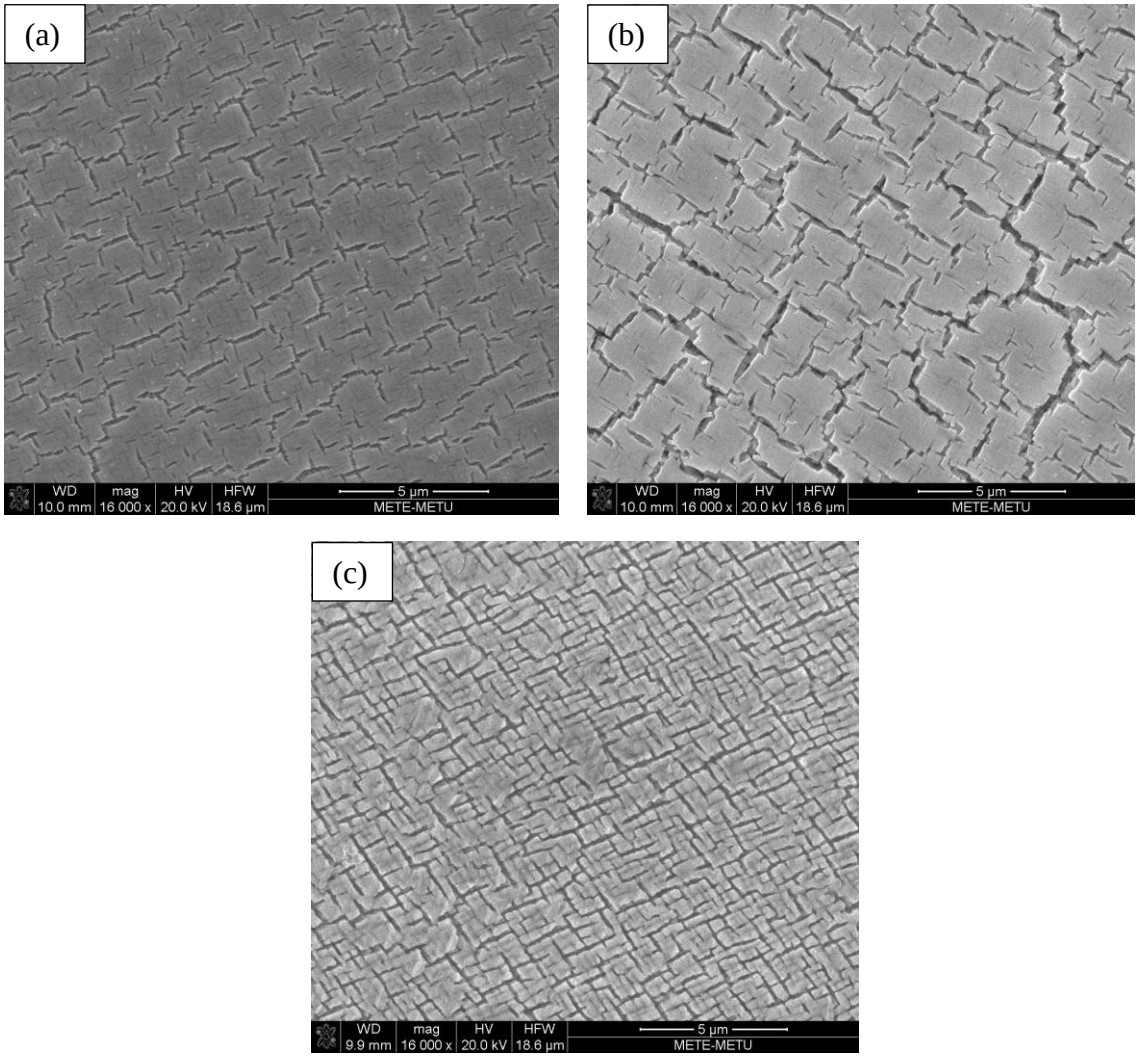

Figure 4-28 FESEM micrographs of aged Co-10Al-9.5W for (a) 16 h, (b) 64 h, (c) 256 h.

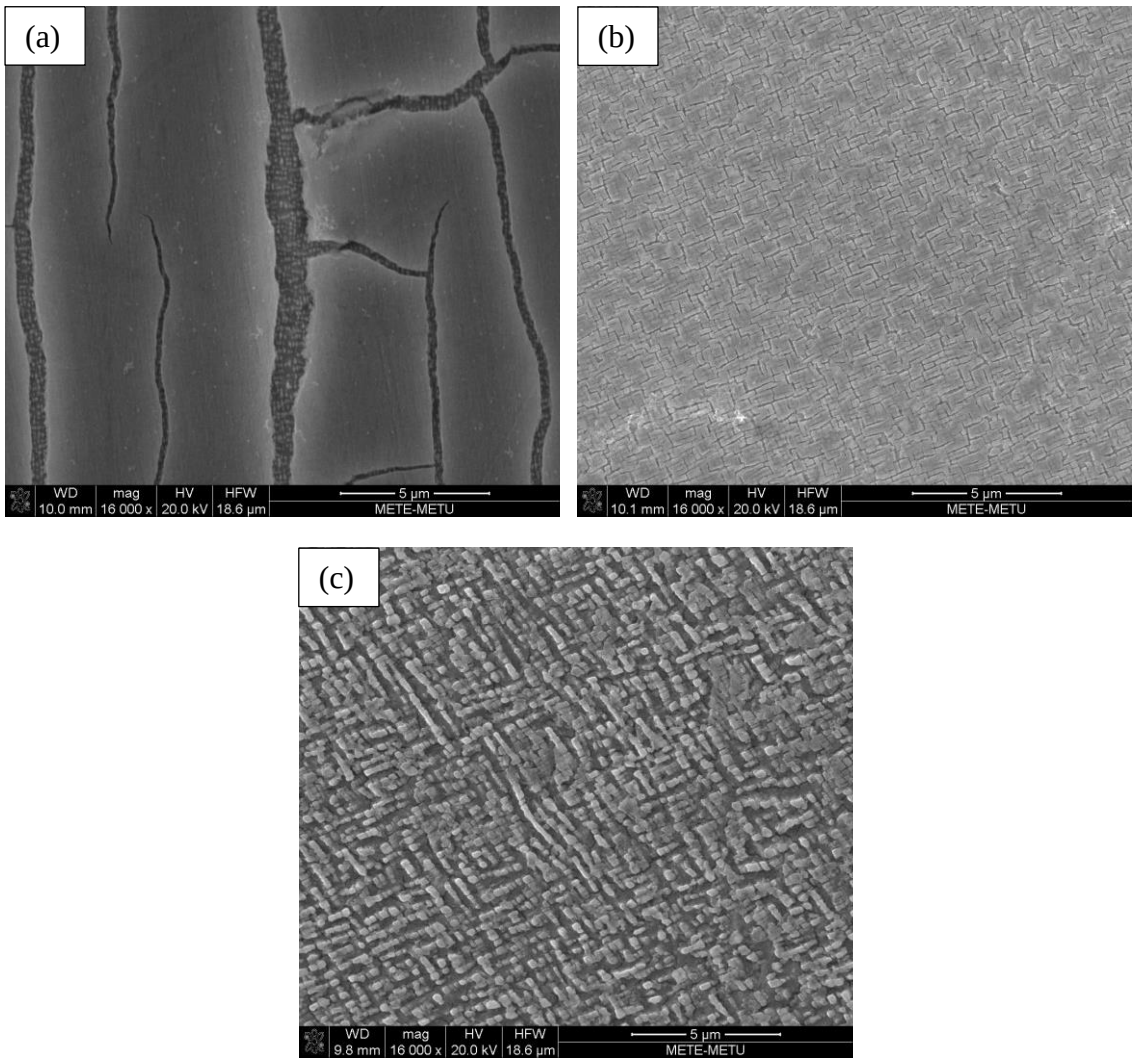

Figure 4-29 FESEM micrographs of aged Co-9Al-7.5W for (a) 16 h, (b) 64 h, (c) 256 h.

Since aging procedure was performed on open atmosphere, inevitable oxidation took place. It had two effects on aged specimens. First of which is a complex oxide layer covered the outer surface of samples. Second of which is a tertiary phase (Co_3W and Co_7W_6) precipitated beneath the oxide layer (Figure 4-30). The reason why γ/γ' dual phase microstructure was disturbed is because Al and W was oxidized in ternary alloys caused

the effective chemical composition deviate from nominal composition. This shift in chemical composition caused needle like Co_3W and globular Co_7W_6 to form. Elemental analyses of both ternary alloys are tabulated in Table 4-4.

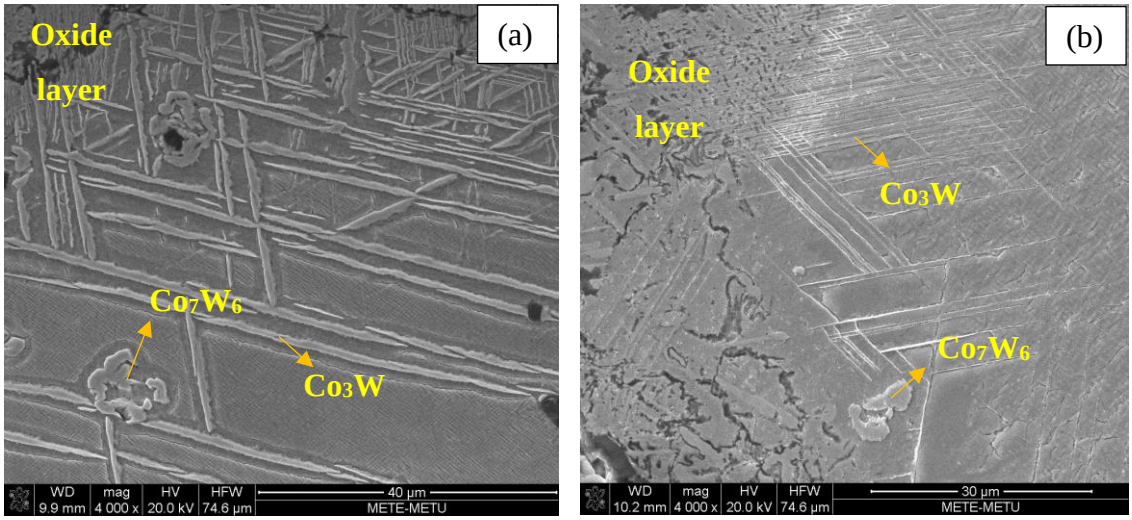

Figure 4-30 Disturbance of γ/γ' two phase region beneath the oxide layer for (a) Co-10Al-9.5W and (b) Co-9Al-7.5W.

Table 4-4 Constituent phases and their elemental analyses for both ternary alloys.

Alloy	Phase	Al at. %	W at. %
Co-9Al-7.5W	γ	8.97	5.72
	γ’	9.21	12.10
	Co_3W	Bal.	25.11
	Co_7W_6	Bal.	47.28
Co-10Al-9W	γ	8.96	5.96
	γ’	9.31	12.31
	Co_3W	Bal.	23.98
	Co_7W_6	Bal.	45.96

4.3.2.3. Microhardness Measurements

Microhardness values were taken to show the effect of heat treatment on mechanical properties (Figure 4-31). It is clear that as the aging time increases hardness values of the ternary alloys goes up. This is due to γ’ formation which is primary deformation prevention mechanism in superalloys. Hardness value of Co-10Al-9.5W alloy is higher than Co-9Al-7.5W alloy as expected because of higher it has higher γ’ fraction than the other.

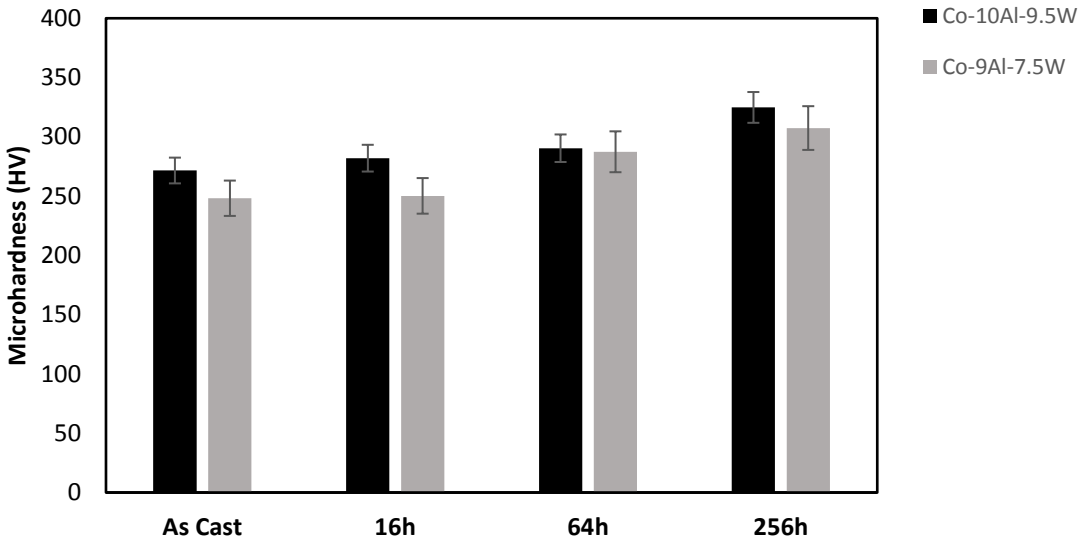

Figure 4-31 Microhardness evolution and comparison of 2 ternary alloys from as cast state to aged condition.

CHAPTER 5

CONCLUSIONS AND FUTURE SUGGESTIONS

5.1. Conclusions

This master thesis has focused on design and development of binary Co_xAl_{1-x} where X = 1.23, 8.40, 16.72, 19.50, 21.50 and 25 & ternary Co-10Al-9.5W and Co-9Al-7.5W alloy systems. For this purpose, aforementioned binary and ternary alloy systems have been produced by arc melting method. Then each binary alloy was given homogenization, ternary alloy was given full solution heat treatment and aging heat treatments at different aging durations to investigate their effect on the microstructural characteristics and temporal evolutions of γ' precipitates. After phase, thermal and microstructural characterizations, mechanical properties of these alloys have been determined by micro-hardness tests.

To sum up what has been found out in this study as follows:

- Co rich side of Co-Al binary solidify in two different ways depending on Al content. Low Al containing alloys that crystallize into fcc-Co from liquid melt show single phase hcp-Co at room temperature. However, it is well known fact that hcp-Co in its equilibrium state holds virtually no Al in its lattice therefore another phase must form. That another phase is β-CoAl, but it did

not exist. It is postulated that metastable hcp-Co that have some Al solubility exist upon solidification and even 24 hours of annealing at 1300 °C was not enough for reaching equilibrium state. Even longer times of annealing is necessary.

- Fcc-Co to hcp-Co transformation can occur via martensitic manner even in slow cooling rates (10 °C /min).
- As-cast and annealed states of high Al containing alloys contained 3 phase state. This tells equilibrium was not reached after 24 hours of annealing at 1300 °C followed by furnace cooling. This state contradicts with Gibbs Phase Rule. Even longer times of annealing is necessary.
- For high Al content alloys, hardness is proportional to Al content. This is due to increasing amount of hard CoAl phase.
- As-cast state of ternary alloys did not agree with equilibrium phase diagram because of very limited diffusion in solid upon solidification.
- Aging of ternary alloys promoted γ/γ' dual phase microstructure for both ternary alloys. As Al & W content increases in ternary alloys, γ' fraction and solvus temperature increases. This also shows itself in hardness measurements where high Al & W containing alloy (Co-10Al-9.5W) has higher hardness than the other (Co-9Al-7.5W).
- While ternary system is mechanically sound, it is extremely sensitive to aggressive environment. Parts where faced oxygen at higher temperatures formed oxides and disturbed γ/γ' microstructure underneath. This sensitivity can be overmatched by Cr addition and TBC coating.

5.2. Future Suggestions

1) TEM investigations can be made in order to further investigate phases in binary alloys.
2) Longer annealing time should be applied to reach equilibrium state for binary alloys.
3) Phase stability of γ' precipitates should be investigated by aging samples very long times such as 1000 hours or more.
4) The effect of transition metal additions (Ni, Ti, Ta, Nb, Cr etc.) on microstructural stability and mechanical properties of γ' can be investigated.
5) In order to reduce weight percent of tungsten, which is a heavy metal, other alternatives need to be researched.
6) The duration of heat treatment procedure of Co-based superalloys should be shortened. 24 hours of solutionizing and many hours of subsequent aging treatment is costly and may not be feasible for industrial applications.
7) Although microhardness values increased for aged alloys when compared to as-cast state, creep testing would be better suited to show the mechanical strength improvement via aging.

REFERENCES

1. Sato, J., et al., *Cobalt-base high-temperature alloys.* Science, 2006. **312**(5770): p. 90-91.
2. Masumoto, H., T. Kobayashi, and K. Watanabe, *On a New Magnet Alloy "Malcolloy" in the System of Cobalt and Aluminum.* Transactions of the Japan Institute of Metals, 1965. **6**(3): p. 187-191.
3. Omori, T., et al., *Shape memory effect in the ferromagnetic Co–14 at.% Al alloy.* Scripta materialia, 2005. **52**(7): p. 565-569.
4. Omori, T., et al., *Shape Memory Effect Associated with FCC—HCP Martensitic Transformation in Co-Al Alloys.* Materials transactions, 2003. **44**(12): p. 2732-2735.
5. Omori, T., et al., *Shape memory and magnetic properties of Co–Al ferromagnetic shape memory alloys.* Materials Science and Engineering: A, 2006. **438**: p. 1045-1049.
6. Koval, Y.N. *High temperature shape memory effect in some alloys and compounds*. in *Materials science forum*. 2000. Trans Tech Publ.
7. Chen, F., et al., *Transformation Behavior and Shape Memory Effect of a CoAl Alloy.* International Journal of Modern Physics B, 2009. **23**(06n07): p. 1931-1936.
8. McAlister, A., *The Al-Co (aluminum-cobalt) system.* Bulletin of Alloy Phase Diagrams, 1989. **10**(6): p. 646-650.
9. Kattner, U. and T. Massalski, *Binary alloy phase diagrams.* ASM International, Materials Park, OH, 1990. **147**.
10. Kimura Y, et al. *Experimental Methods of Phase Diagram Determination*. 1993.
11. Ohtani, H., M. Yamano, and M. Hasebe, *Thermodynamic analysis of the Co–Al–C and Ni–Al–C systems by incorporating ab initio energetic calculations into the CALPHAD approach.* Calphad, 2004. **28**(2): p. 177-190.
12. Stein, F., C. He, and N. Dupin, *Melting behaviour and homogeneity range of B2 CoAl and updated thermodynamic description of the Al–Co system.* Intermetallics, 2013. **39**: p. 58-68.
13. Li, X., et al., *Thermodynamic evaluation of the phase equilibria and glass-forming ability of the Al–Co–Gd system.* Calphad, 2016. **52**: p. 57-65.
14. Guillet, L., *La constitution des alliages [The constitution of alloys]*. Le Génie Civil, 1902. **41**: p. 169-172.

15. Guillet, L., *Contribution à l'étude des alliages d'aluminium*. 1902.
16. Gwyer, A.G., *Über die legierungen des aluminiums mit kupfer, eisen, nickel, kobalt, blei und cadmium.* Zeitschrift für anorganische und allgemeine Chemie, 1908. **57**(1): p. 113-153.
17. Hansen, M., K. Anderko, and H. Salzberg, *Constitution of binary alloys.* Journal of the Electrochemical Society, 1958. **105**(12): p. 260C-261C.
18. Stout, M., T. Courtney, and M. Przystupa, *Redetermination of the invariant compositions in the Co-Coal eutectic.* Metallurgical Transactions A, 1977. **8**(8): p. 1316-1318.
19. Wall, T., W. Predebon, and B. Pletka, *The dependence of yield strength on lamellar termination density in Co-CoAl eutectic alloys.* Acta Metallurgica, 1985. **33**(2): p. 287-294.
20. Köster, W., *Das System Eisen-Kobalt-Aluminium.* steel research international, 1933. **7**(4): p. 263-264.
21. Dupin, N. and I. Ansara, *Thermodynamic assessment of the system Al-Co.* REVUE DE METALLURGIE-CAHIERS D INFORMATIONS TECHNIQUES, 1998. **95**(9): p. 1121-1129.
22. Kimura, Y., et al., *Microstructure control and mechanical properties of binary Co–Al alloys based on B2 intermetallic compound CoAl.* Materials Transactions, JIM, 1994. **35**(3): p. 182-188.
23. Kazantseva, N., et al., *Study of the martensitic transformation in the Co–9 at% Al alloy.* The Physics of Metals and Metallography, 2016. **117**(1): p. 42-48.
24. Williams, R., *Aging of Nickel Base Aluminum Alloys.* TRANSACTIONS OF THE AMERICAN INSTITUTE OF MINING AND METALLURGICAL ENGINEERS, 1959. **215**(6): p. 1026-1032.
25. Zięba, P., G. Cliff, and G.W. Lorimer, *Discontinuous precipitation in cobalt-tungsten alloys.* Acta materialia, 1997. **45**(5): p. 2093-2099.
26. Gust, W., B. Predel, and S. Mehra, *The kinetics of finely lamellar discontinuous precipitation in Co-Mo mixed crystals.* Materials Science and Engineering, 1975. **21**(2): p. 131-138.
27. Lee, S.-L., K.-C. Lee, and T.-H. Chuang, *Discontinuous coarsening of discontinuous precipitates in a Co–6 at.% Mo alloy.* Materials Science and Engineering: A, 1998. **251**(1-2): p. 135-141.
28. Chuang, T., et al., *Discontinuous coarsening of discontinuous precipitate in a Ni-7.5 at.% In alloy.* Acta Metallurgica, 1988. **36**(3): p. 775-785.
29. Geber, G., *An APFIM/TEM investigation of the discontinuous precipitation in a Ni・In alloy.* Applied surface science, 1995. **87**: p. 234-242.
30. Davies, C.K., P. Nash, and R. Stevens, *Precipitation in Ni-Co-Al alloys-Part 1 continuous precipitation.* Journal of Materials Science, 1980. **15**(6): p. 1521-1532.

31. Davies, C.K., et al., *Precipitation in Ni-Co-Al alloys-Part 2 Discontinuous precipitation.* Journal of Materials Science, 1985. **20**(8): p. 2945-2957.
32. Nystrom, J., et al., *Discontinuous cellular precipitation in a high-refractory nickel-base superalloy.* Metallurgical and Materials Transactions A, 1997. **28**(12): p. 2443-2452.
33. Abdou, S., *Discontinuous precipitation, dissolution and coarsening in the Ni±In, Al±Zn and Co±Al systems*. 1987, Ph. D. thesis.
34. Zieba, P., *Microanalytical study of the discontinuous precipitation reaction in a Co–13 at.% Al alloy.* Acta materialia, 1998. **46**(1): p. 369-377.
35. Rojhirunsakool, T., S. Nag, and R. Banerjee, *Discontinuous precipitation of γ′ phase in Ni-Co-Al Alloys.* JOM, 2014. **66**(8): p. 1465-1470.
36. Johnson, R., H. Rayson, and W. Wright, *Factors controlling the coercivity of cobalt-aluminium alloys containing between 20 and 40 at.% aluminium (Malcolloy).* Acta Metallurgica, 1972. **20**(3): p. 387-397.
37. Zeltser, A. and W. Soffa, *Magnetic hardening in Co-Al alloys.* IEEE transactions on magnetics, 1986. **22**(5): p. 588-590.
38. Kozakai, T., T. Koyama, and M. Doi, *Phase decomposition and precipitation of metastable A2 phase in B2 ordered Co–Al–Fe alloys.* Zeitschrift für Metallkunde, 2006. **97**(3): p. 266-272.
39. Kozakai, T., T. Shikama, and T. Koyama. *Metastable two-phase field (A2+ B2) in Co-Al-Fe and Co-Al alloy systems*. in *Materials Science Forum*. 2004. Trans Tech Publ.
40. Kamiya, N., et al., *Phase separation of BCC phase in the Co-rich portion of Co-Fe-Al system.* Intermetallics, 2004. **12**(4): p. 417-423.
41. Ohtani, H., Y. Chen, and M. Hasebe, *Phase separation of the B2 structure accompanied by an ordering in Co-Al and Ni-Al binary systems.* Materials transactions, 2004. **45**(5): p. 1489-1498.
42. Niitsu, K., et al., *Phase transformations in the B2 phase of Co-rich Co–Al binary alloys.* Journal of Alloys and Compounds, 2011. **509**(6): p. 2697-2702.
43. Luo, H.-L. and P. Duwez, *Face-centered cubic cobalt-rich solid solutions in binary alloys with aluminum, gallium, silicon, germanium, and tin.* Canadian Journal of Physics, 1963. **41**(5): p. 758-761.
44. Predel, B., *Al-Co (Aluminum-Cobalt)*, in *Ac-Ag... Au-Zr*. 1991, Springer. p. 1-2.
45. McAlister, A., *Al-Co (Aluminum-Cobalt).* Binary alloy phase diagrams, 1990. **1**: p. 136-138.
46. Nikolin, B. and N. Shevchenko, *New multilayer martensite phases in Co・Al alloys—Polytype structures in metal alloys.* Scripta Metallurgica, 1980. **14**(5): p. 467-472.

47. Widom, M. and E. Cockayne, *Atomic correlations in AlCo decagonal approximant phases.* Physica A: Statistical Mechanics and its Applications, 1996. **232**(3-4): p. 713-722.
48. Sui, H., et al., *The enhancement of solid solubility limits of AlCo intermetallic compound by high-energy ball milling.* Journal of applied physics, 1992. **71**(6): p. 2945-2949.
49. Behm, J.M., D.J. Brugh, and M.D. Morse, *Spectroscopic analysis of the open 3 d subshell transition metal aluminides: AlV, AlCr, and AlCo.* The Journal of chemical physics, 1994. **101**(8): p. 6487-6499.
50. Vedula, K. and J. Stephes, *B2 Alulinides for High Temperature Applications.* MRS Online Proceedings Library Archive, 1986. **81**.
51. Reed, R.C., *The superalloys: fundamentals and applications*. 2008: Cambridge university press.
52. Donachie, M.J. and S.J. Donachie, *Superalloys: a technical guide*. 2002: ASM international.
53. Cacciamani, G., et al., *Critical evaluation of the Fe–Ni, Fe–Ti and Fe–Ni–Ti alloy systems.* Intermetallics, 2006. **14**(10-11): p. 1312-1325.
54. Nash, P., M. Singleton, and J. Murray, *Al-Ni (aluminum-nickel).* Phase diagrams of binary nickel alloys, 1991. **1**: p. 3-11.
55. Bhadeshia, H. and N.-B.S. K D, *University of Cambridge.* IOM communications, 2001.
56. Siebörger, D., et al., *Temperature dependence of lattice parameter, misfit and thermal expansion coefficient of matrix, γ'phase and superalloy.* Zeitschrift fuer Metallkunde, 2001. **92**(1): p. 58-61.
57. Tan, X., et al., *Measurements of γ/γ'Lattice Misfit and γ'Volume Fraction for a Ru-containing Nickel-based Single Crystal Superalloy.* Journal of Materials Science & Technology, 2011. **27**(10): p. 899-905.
58. Tiley, J., et al., *Evaluation of gamma prime volume fractions and lattice misfits in a nickel base superalloy using the external standard X-ray diffraction method.* Materials science and engineering: a, 2010. **528**(1): p. 32-36.
59. Eriş, R., A.O. Mekhrabov, and M.V. Akdeniz, *High-temperature site preference and atomic short-range ordering characteristics of ternary alloying elements in γ'-Ni3Al intermetallics.* Philosophical Magazine, 2017. **97**(29): p. 2615-2631.
60. Eriş, R., M.V. Akdeniz, and A.O. Mekhrabov, *Atomic size effect of alloying elements on the formation, evolution and strengthening of γ'-Ni3Al precipitates in Ni-based superalloys.* Intermetallics, 2019. **109**: p. 37-47.
61. Caron, P. and T. Khan, *Evolution of Ni-based superalloys for single crystal gas turbine blade applications.* Aerospace Science and Technology, 1999. **3**(8): p. 513-523.

62. Harris, K., et al., *Development of the rhenium containing superalloys CMSX-4 & CM 186 LC for single crystal blade and directionally solidified vane applications in advanced turbine engines.* Superalloys 1992, 1992. **297**.
63. Tan, X., et al., *Effect of ruthenium on high-temperature creep rupture life of a single crystal nickel-based superalloy.* Materials Science and Engineering: A, 2011. **528**(29-30): p. 8381-8388.
64. Sugui, T., et al., *Influence of TCP phase and its morphology on creep properties of single crystal nickel-based superalloys.* Materials Science and Engineering: A, 2010. **527**(21-22): p. 5444-5451.
65. Booth-Morrison, C., R.D. Noebe, and D.N. Seidman, *Effects of tantalum on the temporal evolution of a model Ni–Al–Cr superalloy during phase decomposition.* Acta Materialia, 2009. **57**(3): p. 909-920.
66. Amouyal, Y., Z. Mao, and D.N. Seidman, *Combined atom probe tomography and first-principles calculations for studying atomistic interactions between tungsten and tantalum in nickel-based alloys.* Acta Materialia, 2014. **74**: p. 296-308.
67. Floreen, S. and J. Davidson, *The effects of B and Zr on the creep and fatigue crack growth behavior of a Ni-base superalloy.* Metallurgical Transactions A, 1983. **14**(4): p. 895-901.
68. Garosshen, T., T. Tillman, and G. McCarthy, *Effects of B, C, and Zr on the structure and properties of a P/M nickel base superalloy.* Metallurgical Transactions A, 1987. **18**(1): p. 69-77.
69. Chaturvedi, M. and Y.-f. Han, *Strengthening mechanisms in Inconel 718 superalloy.* Metal science, 1983. **17**(3): p. 145-149.
70. Munjal, V. and A. Ardell, *Precipitation hardening of Ni-12.19 at.% Al alloy single crystals.* Acta Metallurgica, 1975. **23**(4): p. 513-520.
71. Raynor, D. and J. Silcock, *Strengthening mechanisms in γ' precipitating alloys.* Metal Science Journal, 1970. **4**(1): p. 121-130.
72. Fleisgher, R., *Solution hardening.* Acta metallurgica, 1961. **9**(11): p. 996-1000.
73. Galindo-Nava, E., L. Connor, and C. Rae, *On the prediction of the yield stress of unimodal and multimodal γ' Nickel-base superalloys.* Acta Materialia, 2015. **98**: p. 377-390.
74. Mishima, Y., et al., *Solid Solution Hardening of Nickel—Role of Transition Metal and B-subgroup Solutes—.* Transactions of the Japan institute of metals, 1986. **27**(9): p. 656-664.
75. Mishima, Y., et al., *Mechanical properties of Ni3Al with ternary addition of transition metal elements.* Transactions of the Japan institute of metals, 1986. **27**(1): p. 41-50.
76. Kozar, R., et al., *Strengthening mechanisms in polycrystalline multimodal nickel-base superalloys.* Metallurgical and Materials Transactions A, 2009. **40**(7): p. 1588-1603.
77. Sims, C.T., N.S. Stoloff, and W.C. Hagel, *superalloys II*. 1987: Wiley New York.

78. Gerold, V. and H. Haberkorn, *On the critical resolved shear stress of solid solutions containing coherent precipitates.* physica status solidi (b), 1966. **16**(2): p. 675-684.
79. Rao §, S., et al., *Discrete dislocation simulations of precipitation hardening in superalloys.* Philosophical Magazine, 2004. **84**(30): p. 3195-3215.
80. Hüther, W. and B. Reppich, *Order hardening of MgO by large precipitated volume fractions of spinel particles.* Materials Science and Engineering, 1979. **39**(2): p. 247-259.
81. Mughrabi, H., *The importance of sign and magnitude of γ/γ′ lattice misfit in superalloys—with special reference to the new γ′-hardened cobalt-base superalloys.* Acta Materialia, 2014. **81**: p. 21-29.
82. Handbook, A., *Alloy phase diagrams.* ASM international, 1992. **3**: p. 2.319.
83. Vander Voort, G. and E. Manilova, *Metallographic Techniques for Superalloys.* Microscopy and Microanalysis, 2004. **10**(S02): p. 690-691.
84. Markström, A., K. Frisk, and B. Sundman, *A revised thermodynamic description of the Co-WC system.* Journal of phase equilibria and diffusion, 2005. **26**(2): p. 152-160.
85. Xue, F., M.L. Wang, and Q. Feng. *Phase Equilibria in Co-rich Co-Al-W alloys at 1300 C and 900 C*. in *Materials Science Forum*. 2011. Trans Tech Publ.
86. Kobayashi, S., et al., *Determination of phase equilibria in the Co-rich Co–Al–W ternary system with a diffusion-couple technique.* Intermetallics, 2009. **17**(12): p. 1085-1089.
87. Tsukamoto, Y., S. Kobayashi, and T. Takasugi. *The Stability of γ'-Co3 (Al, W) Phase in Co-Al-W Ternary System*. in *Materials Science Forum*. 2010. Trans Tech Publ.
88. Lass, E.A., et al., *γ′ Phase stability and phase equilibrium in ternary Co-Al-W at 900 C.* Journal of phase equilibria and diffusion, 2014. **35**(6): p. 711-723.
89. Inui, H., et al. *Mechanical properties of the ternary L12 compound Co3 (Al, W) in single and polycrystalline forms*. in *Advanced Materials Research*. 2011. Trans Tech Publ.
90. Miura, S., K. Ohkubo, and T. Mohri, *Mechanical properties of Co-based L12 intermetallic compound Co3 (Al, W).* Materials Transactions, 2007. **48**(9): p. 2403-2408.
91. Okamoto, N.L., et al., *Plastic deformation of polycrystals of Co3 (Al, W) with the L12 structure.* Philosophical Magazine, 2011. **91**(28): p. 3667-3684.
92. Kobayashi, S., Y. Tsukamoto, and T. Takasugi, *The effects of alloying elements (Ta, Hf) on the thermodynamic stability of γ′-Co3 (Al, W) phase.* Intermetallics, 2012. **31**: p. 94-98.
93. Kobayashi, S., Y. Tsukamoto, and T. Takasugi, *Phase equilibria in the Co-rich Co-Al-W-Ti quaternary system.* Intermetallics, 2011. **19**(12): p. 1908-1912.

94. Yu, J., et al., *A two-stage predicting model for γ′ solvus temperature of L12-strengthened Co-base superalloys based on machine learning.* Intermetallics, 2019. **110**: p. 106466.
95. Omori, T., et al., *Partition behavior of alloying elements and phase transformation temperatures in Co–Al–W-base quaternary systems.* Intermetallics, 2013. **32**: p. 274-283.
96. Ooshima, M., et al., *Effects of quaternary alloying elements on the γ′ solvus temperature of Co–Al–W based alloys with fcc/L12 two-phase microstructures.* Journal of Alloys and Compounds, 2010. **508**(1): p. 71-78.
97. Xue, F., M. Wang, and Q. Feng, *Alloying effects on heat-treated microstructure in Co-Al-W-base superalloys at 1300 C and 900 C.* Superalloys, 2012. **12**: p. 813-821.
98. Bauer, A., et al., *Creep strength and microstructure of polycrystalline γ′–strengthened cobalt-base superalloys.* Superalloys, 2012. **12**: p. 695-703.
99. Bauer, A., et al., *Microstructure and creep strength of different γ/γ′-strengthened Co-base superalloy variants.* Scripta Materialia, 2010. **63**(12): p. 1197-1200.
100. Shinagawa, K., et al., *Phase equilibria and microstructure on γ′ phase in Co-Ni-Al-W system.* Materials transactions, 2008. **49**(6): p. 1474-1479.
101. Yan, H.-Y., V. Vorontsov, and D. Dye, *Alloying effects in polycrystalline γ′ strengthened Co–Al–W base alloys.* Intermetallics, 2014. **48**: p. 44-53.
102. Bauer, A., et al., *Creep properties of different γ′-strengthened Co-base superalloys.* Materials Science and Engineering: A, 2012. **550**: p. 333-341.
103. Bauer, A., et al., *Influence of Iridium on the Properties of γ′-Strengthened Co-Base Superalloys.* Advanced Engineering Materials, 2015. **17**(6): p. 748-754.
104. Yildirim, M., M.V. Akdeniz, and A.O. Mekhrabov, *Effect of ternary alloying elements addition on the order-disorder transformation temperatures of B2-type ordered Fe-Al-X intermetallics.* Metallurgical and Materials Transactions A, 2012. **43**(6): p. 1809-1816.
105. Massalski, T.B., et al., *Binary Alloy Phase Diagrams (ASM International, Materials Park, OH, 1990).* Google Scholar, 1991: p. 3503.
106. Szczotok, A. and B. Chmiela, *Effect of heat treatment on chemical segregation in CMSX-4 nickel-base superalloy.* Journal of Materials Engineering and Performance, 2014. **23**(8): p. 2739-2747.
107. Li, Y., et al., *Microstructure evolution in L1 2 hardened Co-base superalloys during creep.* Journal of Materials Research, 2017. **32**(24): p. 4522-4530.

APPENDICES

A. CALCULATED Co-Al-W TERNARY PHASE DIAGRAMS VARIOUS TEMPERATURES & Co-Al BINARY PHASE DIAGRAM

This appendix shows Co-Al-W ternary phase diagram drawn using Thermo-Calc TCNI9 database.

Phases denoted on phase diagrams and their corresponding phases are given below:

BCC_B2: B2-CoAl

HCP_A3: hcp-Co

MU_PHASE & ALTI3_DO19: Co_3W

FCC_L12: fcc-Co

FCC_L12#2 & FCC_L12#2: $L1_2$-$Co_3(Al,W)$

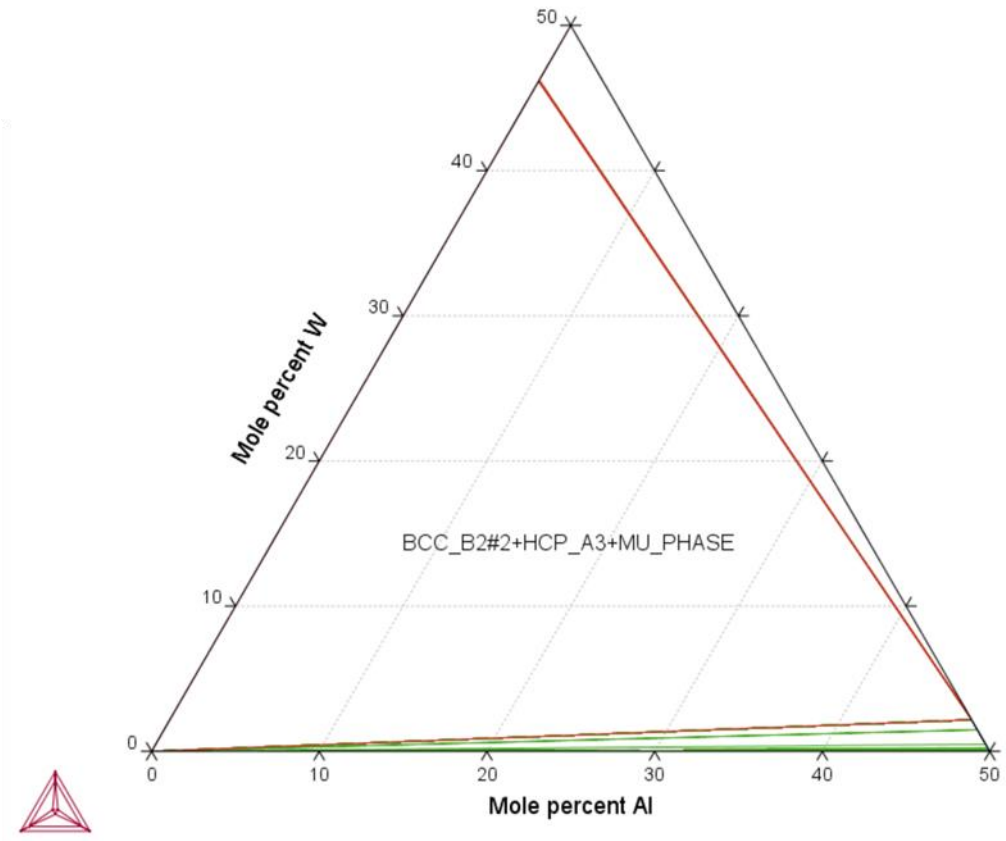

Figure A-1 Co-Al-W ternary phase diagram at 100^0C.

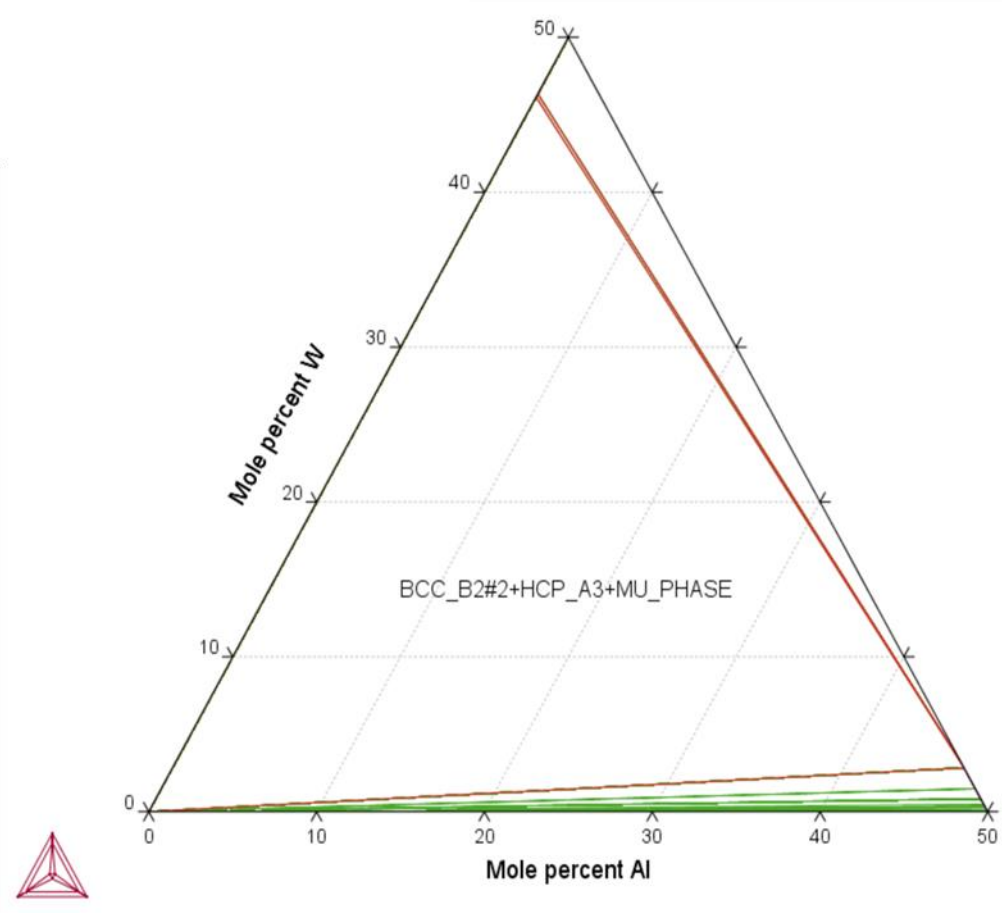

Figure A-2 Co-Al-W ternary phase diagram at 200 °C.

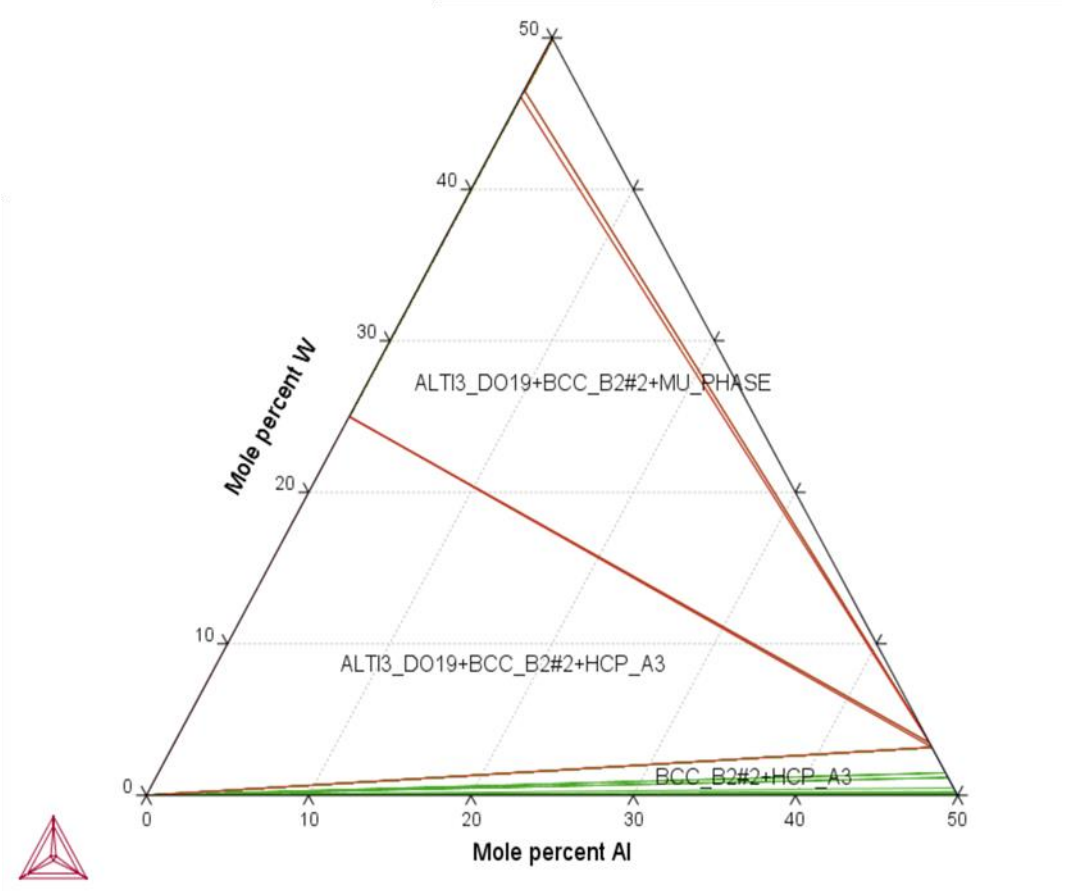

Figure A-3 Co-Al-W ternary phase diagram at 300 °C.

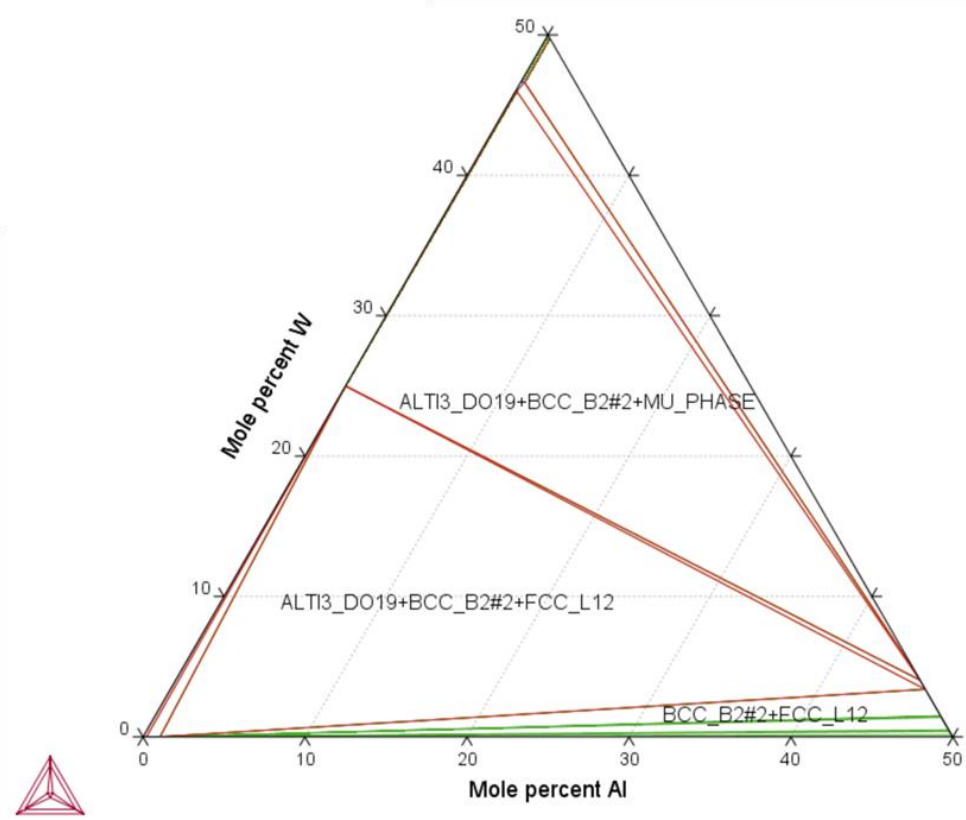

Figure A-4 Co-Al-W ternary phase diagram at 400 °C.

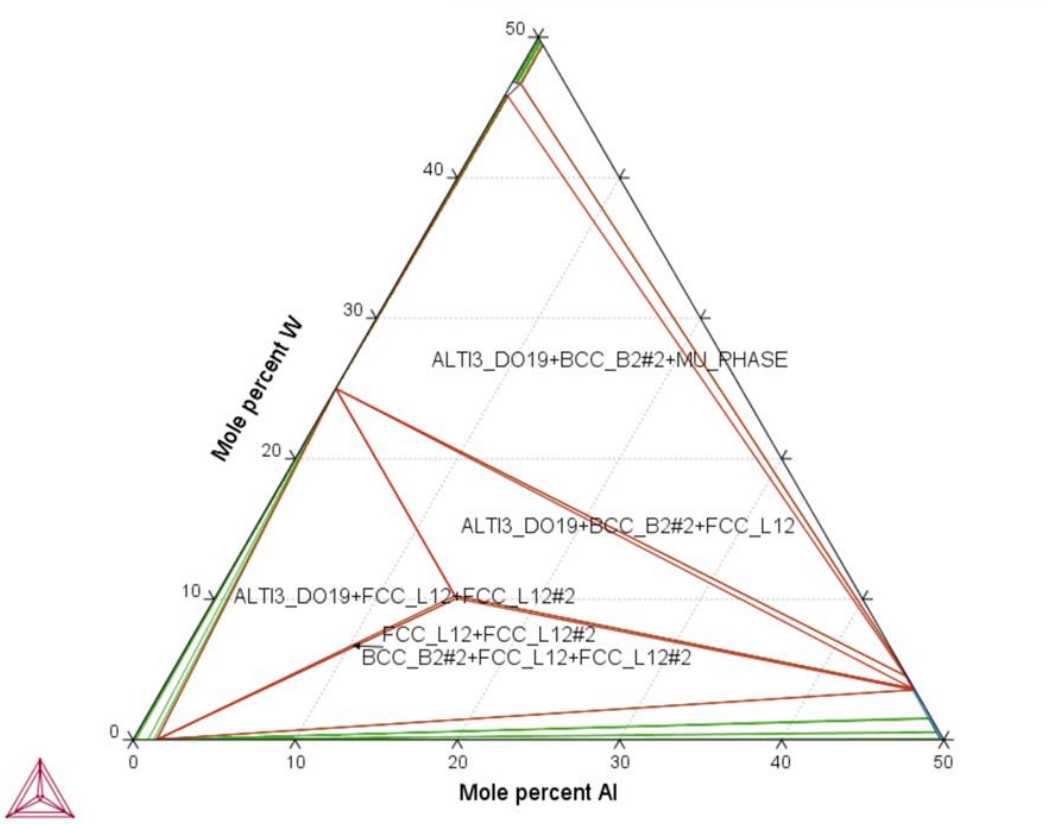

Figure A-5 Co-Al-W ternary phase diagram at 500 °C.

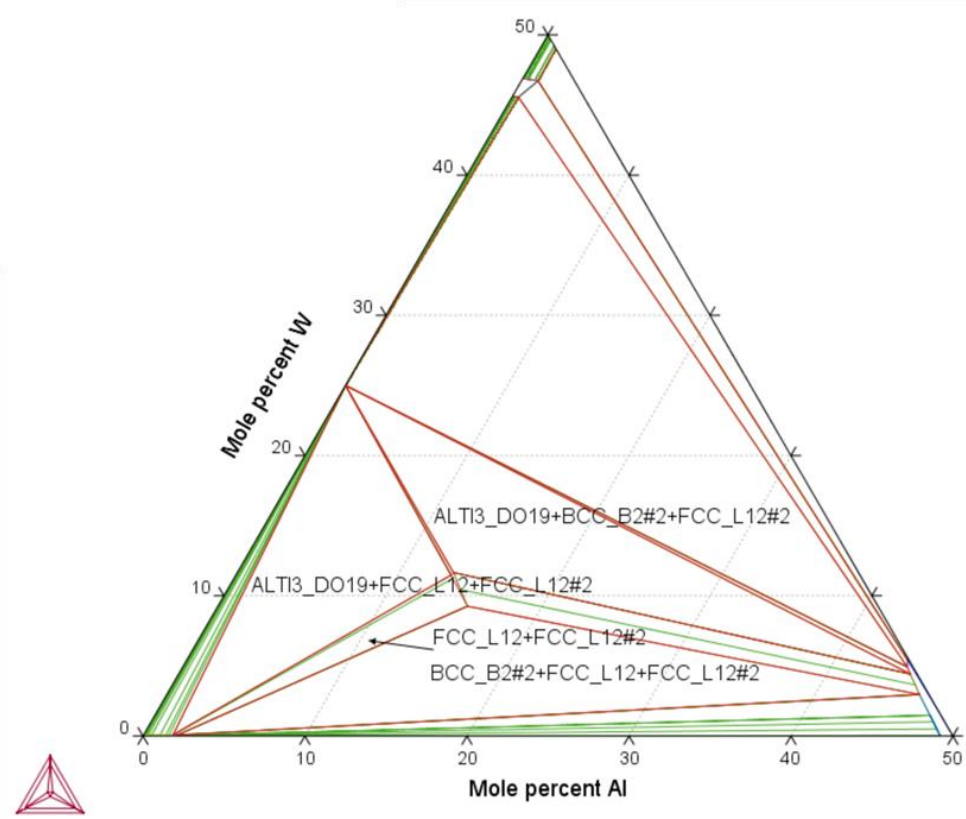

Figure A-6 Co-Al-W ternary phase diagram at 600 °C.

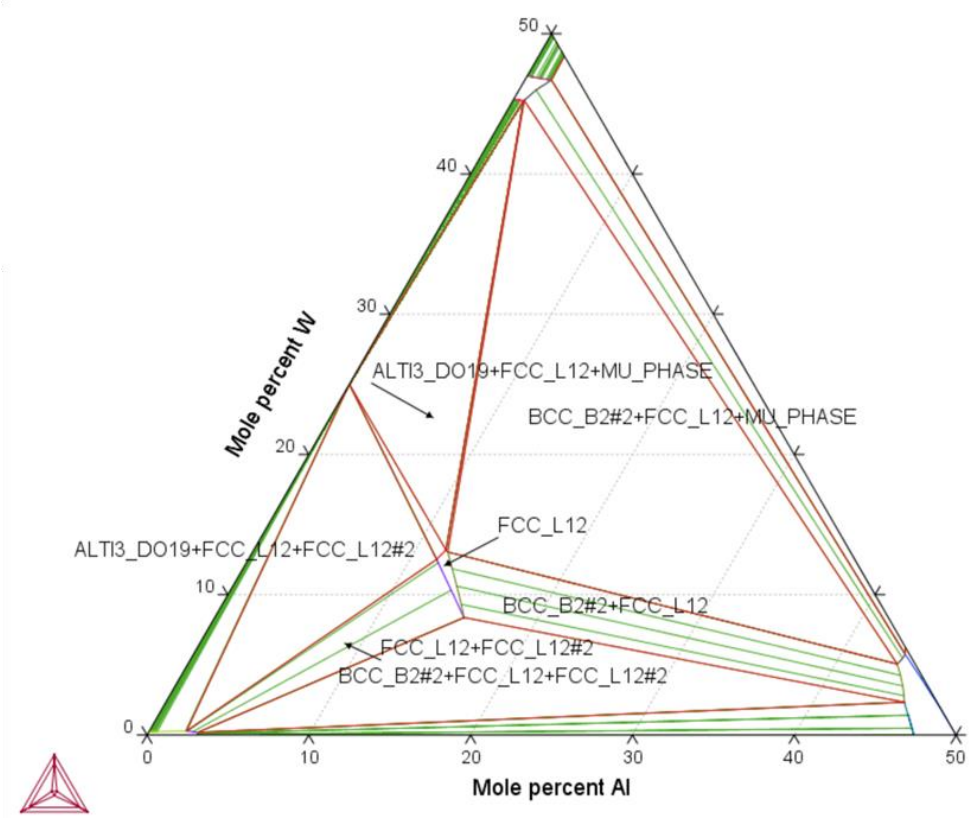

Figure A-7 Co-Al-W ternary phase diagram at 700 °C.

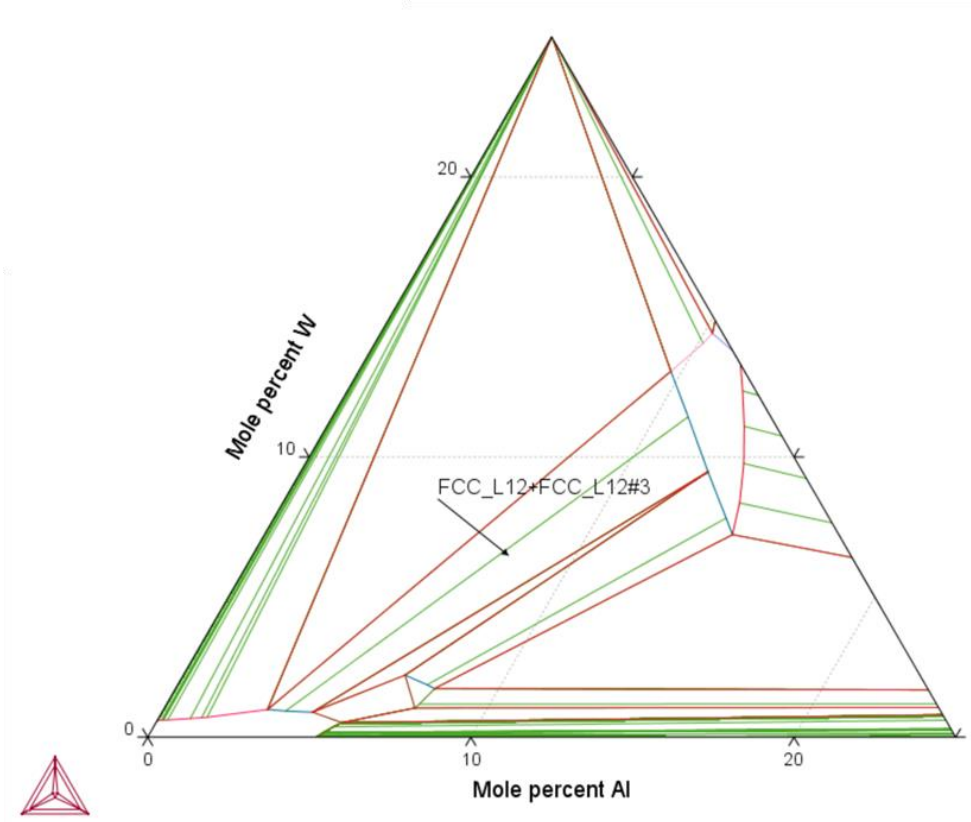

Figure A-8 Co-Al-W ternary phase diagram at 800 °C.

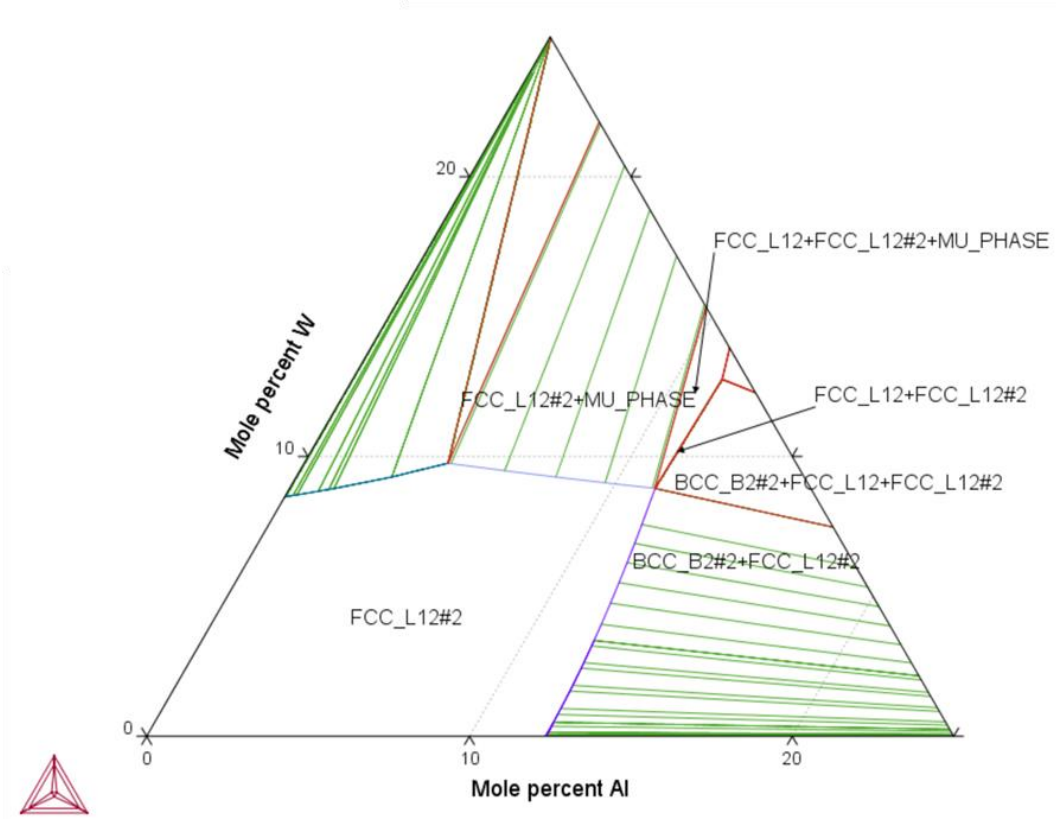

Figure A-9 Co-Al-W ternary phase diagram at 995 °C.

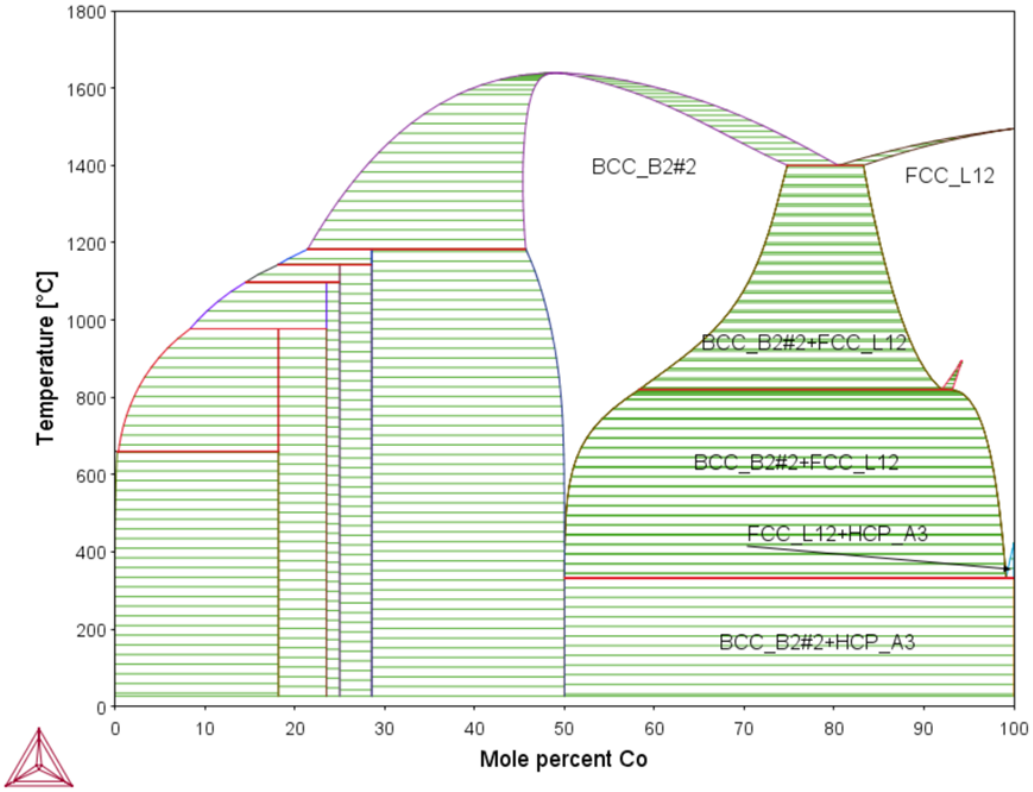

Figure A-10 Co-Al binary phase diagram.